J. Earth Syst. Sci. (2020)129 61
https://doi.org/10.1007/s12040-019-1304-5

Fluvial facies and petrography of Late Pleistocene Baneta sediments, Central Narmada Basin, Madhya Pradesh, India

M G Kale[1], Ashwin S Pundalik[2,*] and Devender Kumar[3]

[1]*Department of Geology, Savitribai Phule Pune University, Pune 411 007, India.*
[2]*Department of Geology, St. Xavier's College, Mumbai 400 001, India.*
[3]*CSIR–National Geophysical Research Institute, Hyderabad 500 007, India.*
**Corresponding author. e-mail: ashwin.pundalik@xaviers.edu*

MS received 19 June 2019; revised 15 September 2019; accepted 26 September 2019

Baneta Formation, comprising of fining upward sequences of pebbly conglomerate, sandstone and siltstone, exhibits development of five distinct lithofacies, viz., massive pebbly conglomerate, large scale tabular cross bedded sandstone, horizontal parallel bedded coarse-grained sandstone, parallel laminated fine-grained yellowish sandstone and siltstone; representing channel lag, point bar and overbank flood plain deposits of mixed load meandering river. In these sediments, development of nodular, buckled bedded calcrete, rhizoliths and tepee is noticed. Granulometric studies of these sediments revealed presence of wide range of grain size classes, polymodal grain size distribution, moderate to very poor sorting, positive skewness and leptokurtic nature, supporting fluvial environment of deposition. Lithic arenitic nature, heavy mineral assemblage with dominance of augite and low ZTR index of these sediments indicate mineralogical immaturity and presence of illite, kaolinite and montmorllionite together with geochemical composition indicate their derivation from mixed provenance of Precambrian granite, metapelites, Vindhyan Supergroup, Gondwana Supergroup, Deccan trap basalt, and laterite. The thin sections studies reveal signatures of meteoric phreatic and vadose zone diagenesis related with semi-arid climate and subaerial exposure. The $\delta^{13}C$ and $\delta^{18}O$ content of calcretes indicate their pedogenic and/or shallow groundwater origin under semi-arid climatic conditions, and C3–C4 mixed vegetation with dominance of C4 vegetation. OSL and ^{14}C dates of the samples from Baneta Formation suggest deposition of these sediments in Late Pleistocene.

Keywords. Quaternary; Narmada; fluvial facies; meandering river; provenance; monsoon; Pleistocene.

1. Introduction

The Central Narmada Basin is one of the few regions of peninsular India where Quaternary deposits are very well developed and preserved. The 1312 km long Narmada River is the largest Indian westerly flowing river into the Arabian Sea (Kathal 2018), which flows through ENE–WSW trending lineament called as Narmada–Son lineament, which has been studied extensively for its structure (e.g., Choubey 1971; Kale 1986; Patro *et al.* 2005). Narmada, Purna and Tapti Basins are the structural basins of central India bounded by North Satpura and South Satpura faults (Vaidyanathan and Ramakrishnan 2008). Reactivation along these faults during Quaternary has given rise to accumulation of about 400 m thick Quaternary deposits in these basins. The Quaternary deposits

Published online: 25 January 2020

of Narmada Basin, due to the presence of rich vertebrate fossil assemblage, artefacts and Younger Toba Ash, have been a subject of extensive paleontological, anthropological and archaeological investigations since early 19th century, along with attempts of paleoclimatic reconstruction based on discovery of several vertebrate fossils including Hominin fossils and artefacts (Splishbury 1833; Tripathi 1968; Badam 1979, 1983; Sonakia 1984; Chauhan and Patnaik 2008; Kotlia and Joshi 2008; Sankhyan *et al.* 2012; Sankhyan 2017).

Several attempts have been made to establish stratigraphy and chronological framework of these deposits based on paleontological, archaeological and geochronological data, presence of Younger Toba Ash and magnetostratigraphy (Theobald 1860; De Terra and Patterson 1939; Biswas *et al.* 1989; Khan and Sonakia 1992; Venkata Rao *et al.* 1997; Patnaik *et al.* 2009). Tiwari and Bhai (1997) have done extensive work on these deposits and they have recognized seven lithostratigraphic formations based on the order of superposition, erosional unconformity, nature of sediments, sedimentary structures, pedogenic characters, presence of tephra and paleomagnetic signature. These are namely Pilikarar Formation, Dhansi Formation, Surajkund Formation, Baneta Formation, Hirdepur Formation, Bauras Formation and Ramnagar Formation in order of decreasing antiquity. Tiwari (2007) correlated various lithostratigraphic formations of Quaternary sediments of Central Narmada basin with Son, Purna, Tapti, Godavari, Vainganga, Mahanadi and river basins of western Maharashtra.

Chamyal *et al.* (2002) carried out geomorphological studies of lower Narmada valley of Gujrat and recognized four geomorphic surfaces namely the alluvial plain (S1), ravine surface (S2), gravelly fan surface (S3), and valley fill terrace surface (S4) within the present landscape; which developed mainly due to tectonic activity along NSF in a compressive stress regime. The sediments comprising S1 and S2 surfaces were deposited in slowly subsiding basin during the Late Pleistocene, which is followed by inversion of basin during the Holocene, marked by differential uplift along NSF; in response to significant increase in compressive stress in Indian Plate during early Holocene. Within these sediments variety of tectonically induced deformational features such as intraformational fold, flexures, slump structures, synsedimentary faults, fractures and joints, and tilting of terraces (S4) were recorded by them. The present incisive drainage and recent seismic activity are the result of continued accumulation of compressive stresses along NSF as a consequence of continued northward movement of Indian Plate (Chamyal *et al.* 2002). Late Pleistocene fluvial sediments now exposed as 30–50 m high incised vertical cliff all along the Lower Narmada valley, were considered to be deposited in a slowly sinking basin (Bhandari *et al.* 2005). They have classified these sediments into two packages, alluvial fan sediments overlain by alluvial plain sediments. The alluvial plain sequence comprises mainly of sand and silt, representing dominance of overbank deposits and large scale sandy bedforms, which were deposited by a low sinuosity large river with high discharge levels, that laterally migrated across the alluvial plain at a high rate; under humid climate conditions. The alluvial plain studies along with underlying alluvial fan sediments suggest that the Narmada River has retained a large catchment to the east since 100 ka (Bhandari *et al.* 2005). Raj (2008) carried out petrographic and geochemical studies of volcanic ash from Quaternary sediments of Madhumati River basin of Lower Narmada basin and correlated with Youngest Toba Tuff of 74,000 ka. Laskar *et al.* (2010) carried out stable C isotopic and radiocarbon dating of surface sediment (depth 0–160 cm) and a paleosol (depth 10–15 m) samples, exposed in Kanjetha cliff section of Lower Narmada valley. According to them, $\delta^{13}C$ of both soil carbonates and soil carbon fall in the range of mixed C3 and C4 vegetation, while paleosol shows differences that can be attributed to contribution from bedrock carbonate during calcite formation. The paleosol was deposited during the Late Pleistocene ($\sim$15–10 ka BP) in more humid climate and the overlying vegetation was dominantly C3. The vegetation was dominantly C3 in Late Pleistocene from $\sim$15 to 10 ka BP, which shifted to mixed C3–C4 during Holocene, providing evidence for significant increase in monsoon rains (Laskar *et al.* 2010). Since $\sim$2.1 ka BP, the climate was semi-arid up to Late Holocene; the replacement of C4 grasses by shrubs and woody plants has been related to anthropogenic disturbance (Laskar *et al.* 2010).

Despite such wide span of literature being available on paleontological, archaeological, anthropological and geochronological aspects of the Quaternary sediments of Central Narmada Basin, sedimentological studies of these sediments have been lacking so far. Fluvial sedimentology is an essential part of terrestrial Quaternary geology, and

a close relationship exists between sedimentary facies association and hydrodynamic conditions prevailing during the sedimentation. According to Chamyal and Juyal (2008), the alluvial tract of peninsular India has remained uninvestigated and there is certainly a need to understand the influence of late Quaternary monsoon variability on hydrology of peninsular rivers. Hence in this paper, we make an attempt to give a detailed account of sedimentation history of Baneta Formation based on the analysis of sedimentary facies and facies association to reconstruct the depositional setting, as well as petrographic studies together with stable isotopic data; to understand the provenance, climatic conditions and paleovegetation during deposition of these sediments.

2. Geological setting

Baneta Formation is the most extensive lithostratigraphic unit of Quaternary succession of Central Narmada basin (figure 1b), and it unconformably overlies Middle Pleistocene Surajkund Formation (Tiwari and Bhai 1997; Patnaik *et al.* 2009). Baneta Formation is studied in detail at river bank cut sections exposed at Hoshangabad, Chandla, Shahaganj, Baneta, North of Baneta, Jahanpur, Surania, Dobi and Narayanpur (figure 1b). It rests unconformably on Proterozoic Vindhyan Supergroup sandstones, Cretaceous–Paleogene Deccan Trap Basalts, Middle Pleistocene Surajkund Formation, and on the top of these sediments, soil cover is developed (figure 1c). Baneta Formation is represented by fining upward sequences of pebbly conglomerate, sandstone and siltstone, which shows development of five distinct lithofacies.

2.1 *Lithofacies description*

2.1.1 *Massive pebbly conglomerate*

Yellowish brown pebbly conglomerate occurs as laterally discontinuous beds in lowermost part of

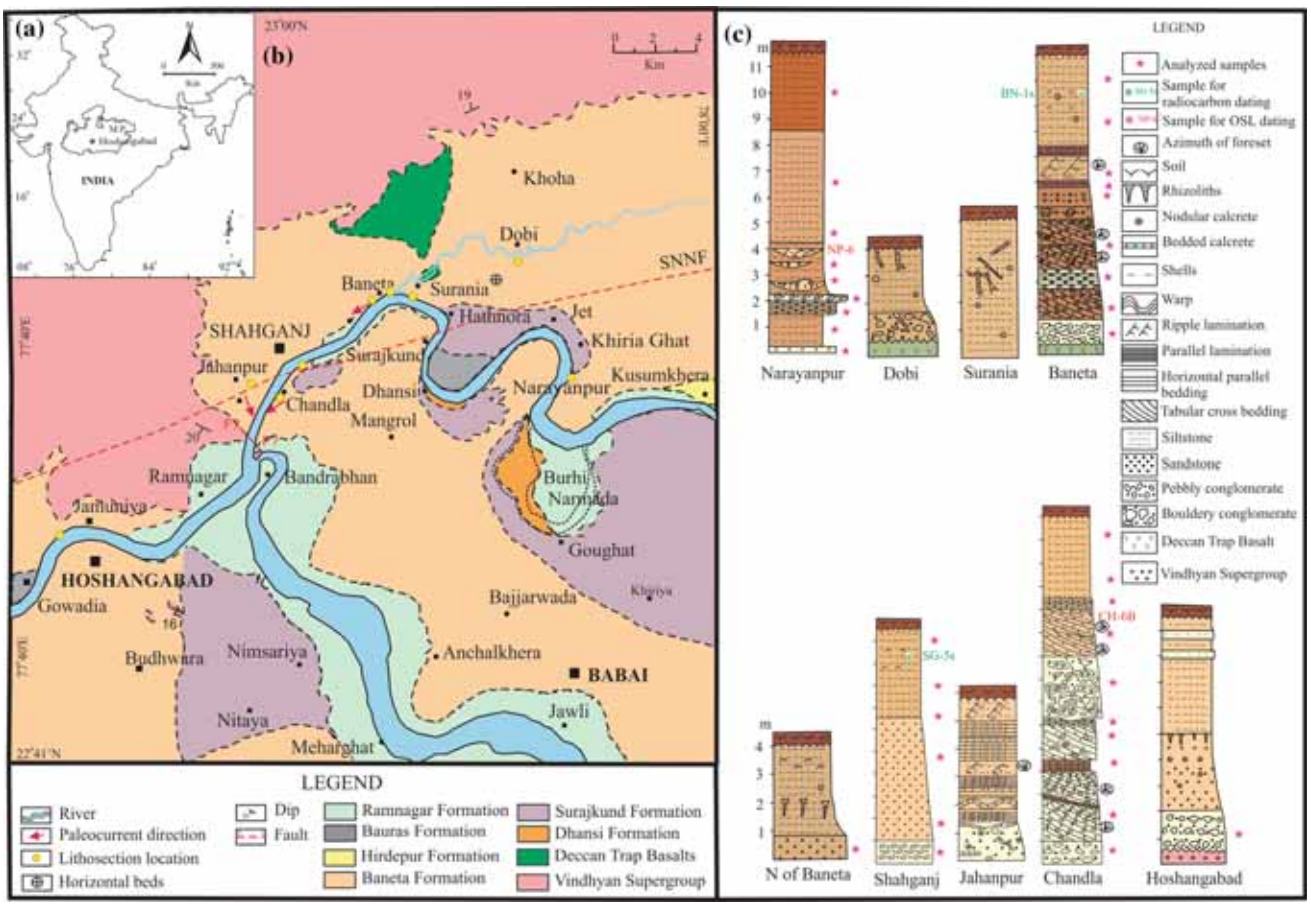

Figure 1. (**a**) Outline map of India showing location of study area. (**b**) Geological map of Baneta area, Central Narmada Basin (modified after Tiwari and Bhai 1997), SNNF: Son Narmada North Fault (after GSI 1993; Mishra 2015). (**c**) Lithosections of Baneta Formation, Central Narmada Basin.

studied lithosections (figure 1c). Its thickness varies from 1 to 2.5 m and it can laterally be traced up to 50 m. In these, dominance of subangular to subrounded pebble size clasts with occasional presence of boulders is noticed. The clasts are of sandstone, vein quartz, agate, jasper, basalt and jaspedious conglomerate, cemented by calcareous cement; hence represent polymictic conglomerate (figure 2a). In the upper part of Chandla lithosection, a variety of this facies representing intra-formational conglomerate is present which is about 2.5 m thick, has scoured erosive irregular contact with horizontal parallel bedded sandstone (figure 2b). It consists of large boulders of calcareous polymictic conglomerate representing recycled clast, which in turn is cemented by calcareous cement (figure 2c). This lithofacies passes upwards into large scale tabular cross bedded coarse-grained sandstone at Chandla and Baneta (figure 1c), and it passes upwards into massive sandstone at Hoshangabad and Shahganj (figure 1c).

2.1.2 *Large scale tabular cross bedded sandstone*

Yellowish brown to brown, coarse- to fine-grained sandstone shows development of large scale tabular cross bedding. It occurs as individual set, as well as coset consisting of number of sets stacked one upon another. The thickness of sets varies from 0.5 to 2 m (figure 2d) and can be laterally traced up to 10 m. The large scale tabular cross bedded sets have planar erosional binding surfaces and are marked by granule layers. Thin layer of parallel laminated siltstone is rarely noticed on top of these binding surfaces (figure 2e). The foresets are of composite nature and show gradation from granule to fine sand and at places presence of brown, elongated pebble size clay galls along the forests is also noticed (figure 2f, g). Occasionally, both lower as well as upper binding surfaces of cross bedded set are observed to be marked with pebbly layer (figure 2g). The foresets of large scale tabular cross beds at different lithosections have a south-westerly directed vector mean. This lithofacies passes upwards into horizontal parallel bedded coarse-grained sandstone at Chandla and Baneta (figure 1c).

2.1.3 *Horizontal parallel bedded coarse-grained sandstone*

This facies is about 0.5 m in thickness and can be laterally traced for 5 m. Generally, this lithofacies overlies and underlies large scale tabular cross bedded sandstone (figure 1c). Horizontal parallel bedding seen to be consisting of alternate granule-rich and granule-poor coarse sand rich layers (figure 2h). On the bedding planes, a network of horizontal burrows is commonly noticed.

2.1.4 *Parallel laminated fine-grained yellowish sandstone*

This facies is developed in the middle and upper parts of Chandla lithosection (figure 1c). The thickness of this facies varies from 30 to 50 cm and can be laterally traced up to 5 m. It overlies large scale tabular cross bedded sandstone. The individual laminae are up to 1 cm in thickness. Occasionally, alternation of laminae of varying thickness consisting of black coloured opaque minerals with non-opaque minerals is noticed. Bioturbation structures represented by vertical burrows are also observed in this sandstone. This sandstone passes upwards into siltstone (figure 1c).

2.1.5 *Siltstone*

Buff-pale to dark brownish siltstone is present in the upper part of all the studied lithosections. Its thickness varies from 0.5 to 7.5 m and is laterally traceable up to 100 m. Within the siltstone, thin streaks as well as layers of carbonaceous clay are also noticed (figure 3a). These siltstones show development of parallel lamination (figure 3b) as well as climbing ripple laminations with inclined nature of sets and truncated upper parts of preceding ripples (Collinson *et al.* 2006) (figure 3c). Sometimes within the siltstones, laterally discontinuous, isolated lenses of better sorted coarse-grained sandstone (figure 1c) occasionally showing ripple lamination are present (figure 3d). These lenses have irregular erosional contact and more or less planar upper contact. Development of rhizoliths within these sandy lenses is also noticed (figure 3d). Within the siltstone, Bivalve shells such as *Parreysia coorgate Muller* (1774), *Lamellidens margainalis Lamarck* (1819) and Gastropod shells such as *Digniostoma cermeopoma Benson* (1830), *Bellamaya bengalensis Lamarck* (1882) and *Thara tuberculata Muller* (1774) (Subba Rao 1989) were noticed (figure 3e).

Within the sediments of Baneta Formation, development of nodular calcrete as well as thin discontinuous, buckled bedded calcrete layers

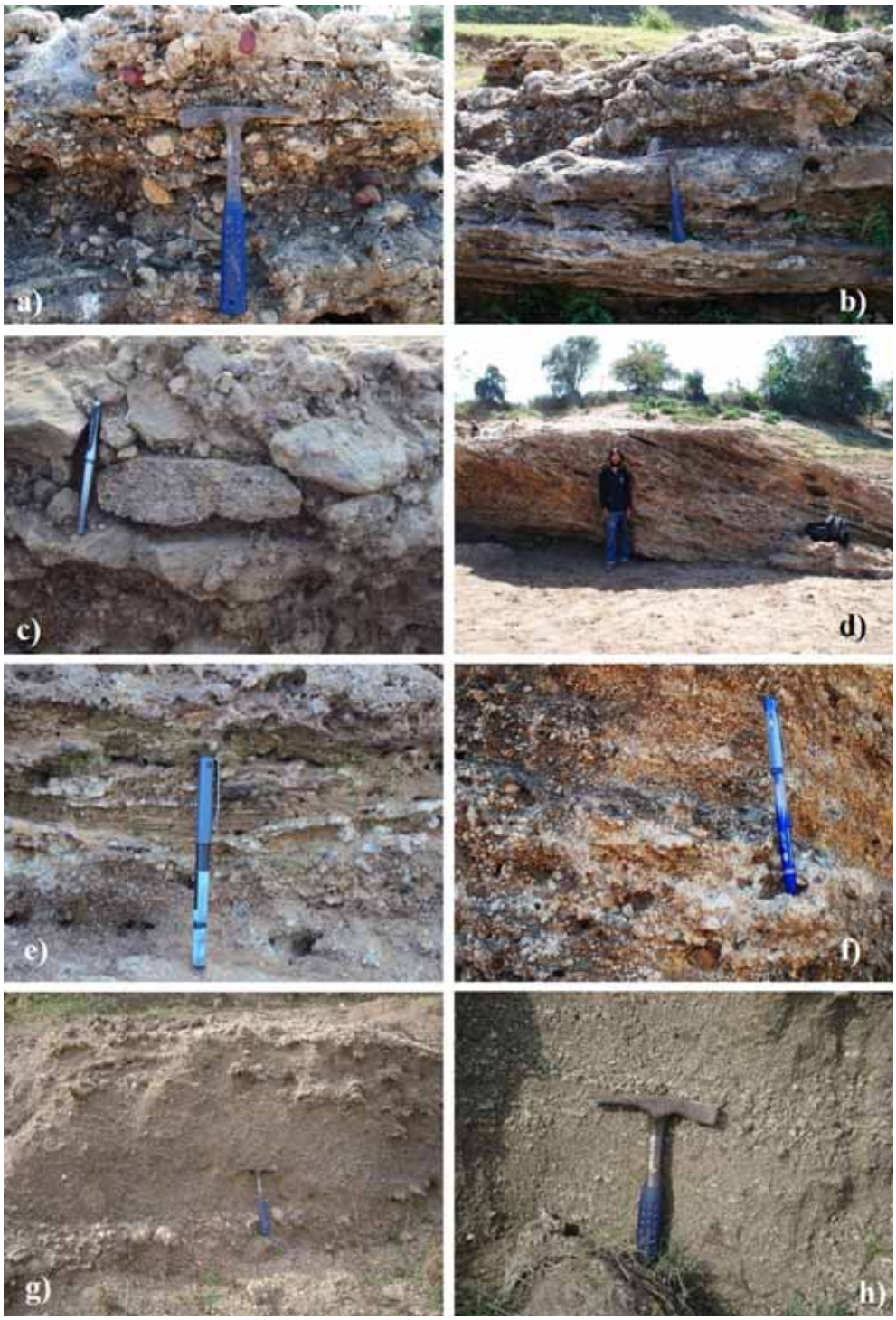

Figure 2. (**a**) Pebbly conglomerate with occasional presence of boulder, consisting of clasts of sandstone, vein quartz, agate and jasper and jasper clast bearing conglomerate cemented by calcareous cement. (**b**) Intraformational conglomerate having scoured irregular contact with horizontal parallel bedded sandstone. (**c**) Close-up view of intraformational conglomerate consisting of slabby, recycled boulder size clasts cemented by calcareous cement. (**d**) Yellowish brown coarse-grained sandstone showing single set of large scale tabular cross bedding having a thickness of 2 m. (**e**) Presence of thin layer of parallel laminated siltstone noticed on top of the binding surfaces of cross bedded sets. (**f**) Composite nature of foresets of large scale tabular cross bedding. Note the presence of brown elongated clay galls along the foresets. (**g**) Coarse-grained sandstone exhibiting large scale tabular cross bedding. Note the presence of large pebble to boulder size pale brownish clay galls in the lower left as well as upper part of this photo. (**h**) Coarse-grained gray sandstone exhibiting horizontal parallel bedding consisting of alternate granule rich and granule poor coarse sand rich layers.

Figure 3. (**a**) Thin streaks and layers of carbonaceous clay within the siltstone. (**b**) Siltstone exhibiting parallel laminations. (**c**) Yellowish buff siltstone exhibiting climbing ripple laminations. (**d**) Laterally discontinuous lenses of better sorted coarse-grained sandstone within the siltstone. (**e**) Presence of bivalve shell in the siltstone. (**f**) Bedded buckled calcrete layer within the siltstone. (**g**) Domed up structure in calcrete representing tepee.

(figure 3f) and rhizoliths are noticed. Occasionally, development of small domed up structures within the calcretes representing tepee (Eren 2007), is also noticed (figure 3g).

3. Laboratory analysis

From the lithosections of Baneta Formation, 37 representative samples of conglomerate, sandstone and siltstone were collected for analysis, out of which 13 well-cemented samples (four samples represent matrix of conglomerate: HB-1, CH-2, SG-1 and BN-1; nine samples are of sandstone: HB-2, HB-3, HB-4, CH-3, CH-4, CH-5, BN-2, BNN-1 and NP-1) were selected for thin section preparation. These were studied under the optical microscope and modal analysis was carried out by using Point counter. Twenty-five samples (Chandla lithosection: 10 samples, Shahganj lithosection: six samples, Baneta lithosection: nine samples) were subjected to granulometric studies by 'Sieve and pipette' method given by Ingram (1971) and Galehouse (1971) respectively, and heavy minerals were separated from fine sand size fraction (2.0 to 4.0 Phi) of 11 samples (Shahganj lithosection: SG-1 to SG-5, Chandla lithosection: CH-1 to CH-6) following method given by Carver (1971). For the separation of clays from samples (matrix of conglomerate: BN-1, CH-2; sandstone: BN-2, BN-3, BN-4, BN-6, CH-4; siltstone: BN-7, CH-8) the fine fraction of insoluble residue of these samples (>4.00 Phi) was transferred to 1000 ml cylinder. After complete dispersal, 100 ml of the sample representing 8.00 Phi was withdrawn at 5 cm depth by using pipette, after 56 min after stirring (Galehouse 1971). The collected clay sample was centrifuged and dried. Thick slurry of clay was prepared and glass slide of requisite dimension, was immersed in the thick slurry so as to get oriented slide prepared. The clay samples were analysed on Phillips X-ray diffractometer by using Cu–K target with a scan range of 4°–70° 2θ, at Wadia Institute of Himalayan Geology, Dehradun.

The geochemical studies of three samples representing matrix of conglomerate, sandstone and siltstone (BN-1, BN-5 and BN-7, respectively) was carried out on XRF (Axios, PAN analytical) and ICP-MS (ThermoX series 2) at National Institute of Oceanography, Goa. Loss on Ignition (LOI) was determined at Wadia Institute of Himalyan Geology, Dehradun. For these samples, weathering indices such as CIA, i.e., chemical index of alteration ($(Al_2O_3/Al_2O_3 + Na_2O + K_2O + CaO^*) \times 100$; Nesbitt and Young 1982), PIA, i.e., plagioclase index of alteration ($[(Al_2O_3 - K_2O)/((Al_2O_3 - K_2O) + CaO^* + Na_2O)] \times 100$; Fedo *et al.* 1995), CIW, i.e., chemical index of weathering ($[Al_2O_3/(Al_2O_3 + CaO^* + Na_2O)] \times 100$; Harnois 1988), a modified version of CIW, i.e., CIW′ for carbonate-bearing siliciclastic rocks ($[Al_2O_3/(Al_2O_3 + Na_2O)] \times 100$; Cullers 2000), ICV, i.e., index of compositional variability ($(Fe_2O_3 + K_2O + Na_2O + CaO + MgO + MnO + TiO_2)/Al_2O_3$; Cox *et al.* 1995), WIP, i.e., weathering index ($100 \times (CaO^*/0.72 + 2Na_2O/0.35 + 2K_2O/0.25 + MgO/0.9)$; Parker 1970) and W index ($\exp(0.203\ln(SiO_2) + 0.191\ln(TiO_2) + 0.296\ln(Al_2O_3) + 0.215\ln(Fe_2O_3) - 0.002\ln(MgO) - 0.448\ln(CaO^*) - 0.464\ln(Na_2O) + 0.008\ln(K_2O) - 1.374)$; Ohta and Arai 2007) were calculated. Stable isotope composition of 14 samples of *in-situ* formed nodular calcrete, bedded calcrete and rhizoliths (table 4) was determined at CSIR–National Institute of Geophysical Research, Hyderabad, using Thermo Finnigan Delta plus XP Continuous Flow Isotope Ratio Mass Spectrometer (CF-IRMS) with attached preparation device Gas Bench II and robotic sampling arm (CG-PAL). Using the $\delta^{18}O$ values and following the procedure given by Friedman and O'neil (1977), the temperature for calcite precipitation was calculated. With the help of $\delta^{13}C$ values, the value of pCO_2 for the samples was estimated following method of Cerling (1999). Two mollusc shell samples (SG-5 s and BN-1 s; sample positions – figure 1c) from the area under study were subjected to radiocarbon dating by Liquid Scintillation Counter (LSC) at Birbal Sahni Institute of Palobotany, Lucknow; using the procedure of Nautiyal (2012). OSL measurements of two samples (CH-6B and NP-6) were carried out using an automated Riso TL/OSL reader (model TL-DA-15, Bøtter-Jensen *et al.* 2003) at CSIR–NGRI, Hyderabad. The samples were collected in opaque cylindrical aluminium tubes with the standard sampling precautions. Quartz grains (150–250 μm) were extracted using a sequential treatment of samples with 1 N HCl and 30% H_2O_2 followed by sieving and etching with 40% HF under subdued red-light conditions. For optical stimulation of quartz, blue LEDs (470 ± 30 nm) were used and the detection of the OSL signal was through a 7-mm Hoya U-340 filter. All OSL measurements were performed using a SAR protocol (Wintle and Murray 2000) for equivalent dose (De) estimation. Annual dose rates were calculated from the elemental concentrations

(measured using ICP-MS and XRF) of U, Th and K (Aitken 1998).

4. Results

4.1 *Thin section studies*

In the thin sections (four samples represent matrix of conglomerate: HB-1, CH-2, SG-1 and BN-1, nine samples are of sandstone: HB-2, HB-3, HB-4, CH-3, CH-4, CH-5, BN-2, BNN-1 and NP-1), framework constituents present are quartz (av. 30.65%), unstable lithic fragments (av. 13.24%), feldspar (av. 4.10%), clay pellets (av. 0.74%), mica (av. 0.41%), volcanic glass (av. 0.31%), pyroxene (av. 0.24%), accessories represented by hornblende, magnetite and ilmenite (av. 0.41%), bounded by calcium carbonate cement (av. 49.90%), hence represent lithic arenite (figure 4a); indicating their mineralogically immature nature (Okada 1971). On Dickinson's (1985) classification diagram (figure 4b), these sediments show derivation from quartzose recycled and transitional recycled provenance. Within quartz, monocrystalline quartz (av. 21.28%) well dominates the polycrystalline quartz (av. 9.38%). Quartz grains vary in size from silt to coarse sand with dominance of medium to coarse sand, with a few granule size grains. Majority of the grains are subangular to subrounded in nature. Commonly, within the quartz grains, presence of cracks filled with either calcareous cement or clay is noticed and inclusions of micritic calcite, clay, and pyroxene are also observed in some grains. Different varieties of polycrystalline quartz grains present are polycrystalline grain consisting of three constituent grains of different size with irregular grain contacts (figure 5a-i), gneissic quartz with varying size elongated quartz grains with preferential orientation and sutured grain contacts (figure 5a–ii and iii), grain consisting of large number of varying size grains with irregular contacts (figure 5a–iv), grain with large number of varying size grains with interlocking arrangement (figure 5a–v), rounded polycrystalline quartz with equant grains showing interlocking arrangement (figure 5a–vi), grain consisting of large number of varying size grains with irregular contacts (figure 5a–vii), grain with inclusion of rounded zircon (figure 5a–viii), coarse sand size elongated fine-grained chert fragment (figure 5a–ix), fibrous chalcedony fragment with fan shaped radiating fibrous crystals (figure 5a–x), well-rounded fragment consisting of concentric laminations of alternating crystalline and cryptocrystalline silica developed around fine grained crystalline core (figure 5a–xi), and red banded jasper fragment (figure 5a–xii). Within feldspars, K-feldspar (av. 2.47%) predominates over plagioclase feldspar (av. 1.63%). Different unstable rock fragments (figure 5b–i to xviii) present in these thin sections are varieties of siltstone, carbonaceous and ferruginous sandstone, laterite, granite, granodiorite, fresh as well as weathered basalt, phyllite and mica gneiss. In general, in these thin sections, micritic calcite cement (av. 26.18%) dominates over the sparry calcite cement (av. 23.72%). Micritic calcite occurs in the form of thin isopachous rims around the framework grains (figure 6a), as well as well-developed caliche

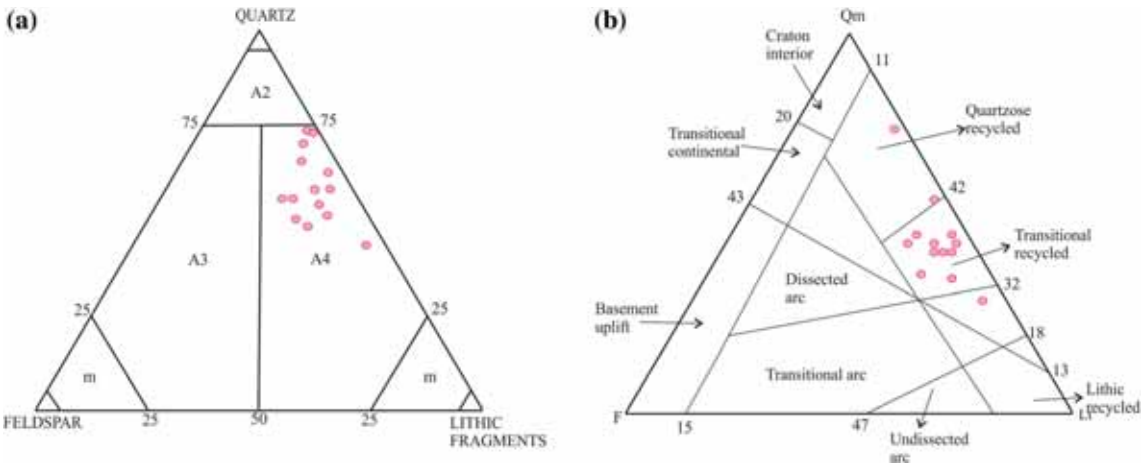

Figure 4. (**a**) Triangular diagram showing composition of sediments of Baneta Formation (after Okada 1971). A1: Quartz arenite, A2: Quartzose arenite, A3: Feldspathic arenite, A4: Lithic arenite and m: monomineralic field. (**b**) QmFLt Ternary diagram for sediments of Baneta Formation (after Dickinson 1985).

nodules of varying size and shape (figure 6b), which are mostly devoid of any nucleus. Development of circumgranular cracks and infiltration of carbonaceous clay along the cracks is observed within these caliche nodules, and at places the nodules are partially surrounded by carbonaceous clay. Within some of the caliche nodules, detrital grains of quartz, jasper, feldspar, glass, laterite, and opaques are noticed, representing recycled caliche nodule (figure 6c). In such recycled caliche nodules, partial as well as complete development of micritic calcite rim around the detrital grains is noticed and the nodule is in turn surrounded by bladed blocky calcite (figure 6c). These caliche nodules and other framework constituents are floating in sparry calcite cement. In many thin sections, intergranular as well as intragranular pore space is occupied by dense crystalline mosaic of sparry calcite. The sparry calcite cement also occurs as isopachous layers of bladed blocky calcite surrounding the micritic caliche nodule as well as the framework grains and in such cases blocky sparry calcite crystals directly abut against grain boundaries. In these thin sections, development of irregular fenestrae, partially or completely filled with microspar or sparry calcite is noticed (figure 6d). These fenestrae are associated with alveolar texture. In some thin sections, pedotubules occurring as irregular interconnected pores formed by rootlet penetration and decay, marked by organic matter are noticed (figure 6e). Rhizoliths exhibit total disruption of original depositional texture and micritization of adjacent sediment and root channel ways partly lined with pale brownish black clay are also seen (figure 6f).

4.2 *Granulometric studies*

Sediments of Baneta Formation exhibit of wide range of grain size classes ranging from −5.50 to >10.0 Phi, polymodal grain size distribution, moderate to very poor sorting (av. 1.93 Phi), positive skewness (av. 0.27 Phi) and moderately to strongly leptokurtic nature (av. 1.52 Phi) related with mixing of two or more subequal grain size populations. The log probability plots (Visher 1969) of these sediments show better-sorted saltation as well as surface creep population, and poorly sorted suspension population, in which the truncation point between surface creep and saltation population (T1) lies between −1.9 and 0.2 Phi and truncation point between saltation and suspension population (T2) lies between 2.2 and 5.2 Phi.

4.3 *Heavy mineral and X-ray diffraction studies*

The frequency percentages of transparent heavy mineral species present in the sediments of Baneta Formation are given in table 1. The heavy mineral assemblage of Baneta Formation is predominated by augite along with zircon, tourmaline, rutile, epidote, staurolite, garnet sillimanite, kyanite, sphene, spinel, chlorite, monazite, hornblende and anatase; with very low ZTR index (Hubert 1962) of av. 4.10. In general, augite (av. 85.98%) dominates and constitutes 2/3 of the heavy mineral crop. For these sediments, various provenance sensitive indices of Morton and Hallsworth (1994, 1999) and Morton and Milne (2012) were calculated, and the values of these indices are given in table 1. The samples from Baneta Formation show high values of GZi, GtZRT, RZi and UTi, moderate values of CZi and SZi, and low values of RuZi, MZi, AmZRT, EpZRT, GtZRT and KyZRT owing to high proportion of pyroxene in heavy mineral crop as well as low value of ZRT index. X-ray diffractograms of the clays from Baneta Formation reveal the presence of illite (3.42 dÅ – 100%, 3.35 dÅ – 51% to 100%, 3.34 dÅ – 100%, 3.33 dÅ – 100%, 2.45 dÅ – 16%), and kaolinite (4.48 dÅ – 25%) with minor montmorillonite (4.45 dÅ – 32%).

4.4 *Geochemical studies*

The obtained values of major oxides (weight percentages), trace element composition (ppm) and chondrite normalized rare earth element composition (ppm) of Baneta sediment samples are given in tables 2 and 3, respectively. The sediments from Baneta Formation show high values of Fe_2O_3/K_2O as compared to Na_2O/K_2O due to their low feldspar content and high proportion of basaltic rock fragments (Pettijohn *et al.* 1972; Herron 1988). On major oxide provenance discrimination diagrams of Roser and Korsch (1988), samples from Baneta Formation show mixed provenance, i.e., quartzose sedimentary, intermediate igneous and mafic igneous (figure 7a and b). On the A–CN–K ternary diagram of Nesbitt and Young (1984, 1989) and CaO^*–(Al_2O_3 + K_2O)–Na_2O plot of Fedo *et al.* (1995) (figure 7c and d), sediments from Baneta Formation exhibit moderate to intense weathering of source rock as well as plagioclase feldspars respectively. CIA and CIW are used to evaluate weathering of sediment source (Nesbitt and Young 1982; Harnois 1988),

PIA estimates degree of plagioclase alteration (Fedo *et al.* 1995), CIW′ is used as measure of source weathering for carbonate bearing siliciclastic rocks (Cullers 2000), ICV is used to evaluate mineralogical maturity (Cox *et al.* 1995), WIP and W index to determine the degree of recycling (Parker 1970; Ohta and Arai 2007). These weathering indices in combination are used to evaluate weathering of source, nature of source as well as mobility of elements during diagenesis and leaching (Jafarzadeh and Hosseini-Barzi 2008). The obtained values of these weathering indices are given in table 2. For discriminating tectonic set-up of sediment deposition, Verma and Armstrong-Altrin (2013) have proposed a new discriminant-function-based multi-dimensional diagram in which sediments under study plot within the continental rift field (figure 7e(i)). On major and trace oxide discrimination diagrams of Verma and Armstrong-Altrin (2016), samples from Baneta Formation plot in passive margin field (figure 7e(ii)).

The sediments from Baneta Formation show a general enrichment in transition trace elements and depletion in HFSEs (table 3, figure 8a). Concentration of transition trace elements, LILE and HFSE increases with decrease in grain size (table 3).The chondrite normalized (Lodders and Fegley 1998) rare earth element composition of sediments under study is given table 3 and the prepared plots are exhibited in figure 8(b). The fractionated REE pattern of these sediments is characterized by high values (av. 8.68) of La/Yb ratio (Xie *et al.* 2017). These sediments exhibit enriched LREE (La/Sm 3.09–4.26) (Banerjee and Banerjee 2010) and depleted HREE (LREE/HREE < 1), negative europium anomaly and weakly positive Ce anomaly (figure 8b).

4.5 *Stable isotope studies*

The obtained values of stable isotopes of oxygen and carbon are given in table 4. The calculated paleotemperature of precipitation for calcretes and rhizoliths from Baneta Formation ranges from 25.09° to 35.16 °C, and average 31.70 °C (table 4). The $\delta^{13}C$ of soil carbonates has been used as a proxy for estimating paleoatmospheric pCO_2 (Cerling 1999; Ekart *et al.* 1999; Robinson *et al.* 2002). The calculated value of pCO_2 for calcretes from Baneta Formation ranges between 197.2 and 1349.7 ppmV and average 656.2 ppmV (table 4).

4.6 *Radiocarbon dating*

The shell samples from Baneta Formation yielded Late Pleistocene age as revealed by the radiocarbon date of 22.63 ± 0.44 ^{14}C ka of sample BN-1s from upper part of Baneta lithosection and date of 17.05 ± 0.93 ^{14}C ka of sample SG-5s from upper part of Shahganj lithosection.

4.7 *OSL dating*

OSL dating of sample from lower part of Narayanpur lithosection (NP-6) gave an age of 83.72 ± 6.94 ka (measured in 2014 AD) and sample from upper part of Chandla lithosection (CH-6B) gave an age of 82.36 ± 8.06 ka (measured in 2014 AD). Hence, both the samples belong to Late Pleistocene Epoch (Gibbard *et al.* 2010).

Figure 5. (**a**) (i) Polycrystalline grain consisting of three constituent grains of different size with irregular grain contacts. (ii and iii) Gneissic quartz with varying size elongated quartz grains with preferential orientation and sutured grain contacts. (iv) Polycrystalline quartz grain consisting of large number of varying size grains with irregular contacts. (v) Rounded polycrystalline quartz with large number of varying size grains with interlocking arrangement. (vi) Rounded polycrystalline quartz with equant grains showing interlocking arrangement. (vii) Polycrystalline quartz grain consisting of large number of varying size grains with irregular contacts. (viii) Polycrystalline quartz with inclusion of rounded zircon. (ix) Coarse sand size elongated fine-grained chert fragment. (x) Fibrous chalcedony fragment with fan shaped radiating fibrous crystals. (xi) Well-rounded fragment consisting of seven concentric laminations of alternating crystalline and cryptocrystalline silica developed around fine grained central crystalline core. (xii) Yellowish red banded jasper fragment. (**b**) (i) Medium sand size subrounded pale brownish siltstone containing silt size quartz grains floating in pale brownish matrix. (ii) Coarse sand size carbonaceous siltstone consisting of silt size angular to subangular quartz grains floating in carbonaceous clay. (iii) Coarse sand size subrounded fragment of fine grained carbonaceous sandstone, consists of angular to subrounded framework grains floating in carbonaceous clay. (iv) Medium sand size fragment of ferruginous sandstone consisting of poorly sorted framework grains floating in pale brownish ferruginous cement. (v) Subrounded reddish brown laterite fragment showing concretionary nature. (vi) Medium sand size, subrounded granitic rock fragment consist of microcline containing subrounded to well-rounded quartz inclusions. (vii) Coarse sand size granitic rock fragment consists of intergrowth of quartz and microcline Feldspar. (viii) Medium sand size granodiorte fragment consisting of microcline, pyroxene, quartz, and plagioclase. (ix–xvi) Varieties of basalt fragments. (xvii) Coarse sand size elongated brownish phyllite fragment. (xviii) Medium sand size fragment of mica gneiss consist of comparatively thick quartz layers with sutured grain contacts alternating with mica rich layers.

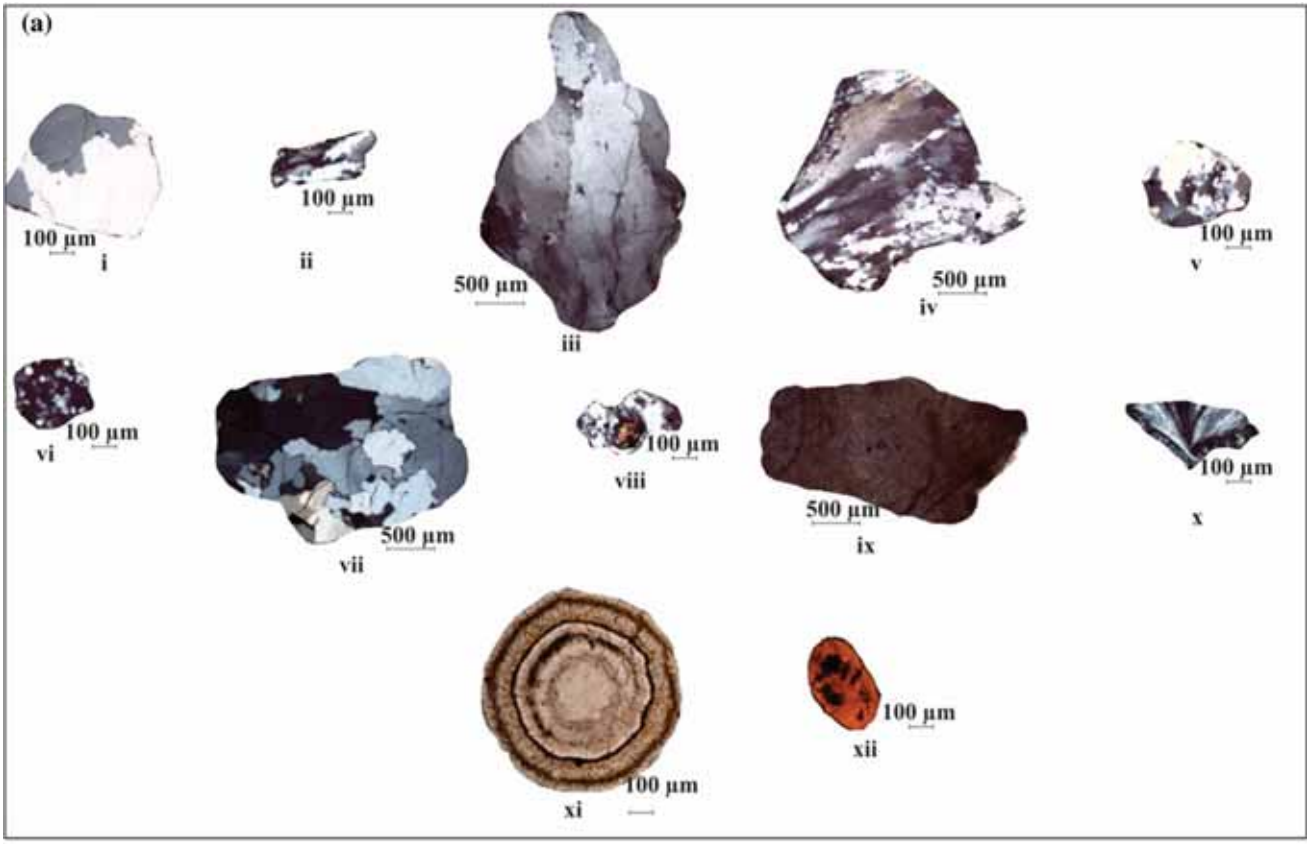
(a)
100 µm
i
100 µm
ii
500 µm
iii
500 µm
iv
100 µm
v
100 µm
vi
500 µm
vii
100 µm
viii
500 µm
ix
100 µm
x
100 µm
xi
100 µm
xii


(b)
100 µm
i
500 µm
ii
500 µm
iii
100 µm
iv
100 µm
v
100 µm
vi
500 µm
vii
100 µm
viii
100 µm
ix
500 µm
x
100 µm
xi
100 µm
xii
100 µm
xiii
100 µm
xiv
500 µm
xv
500 µm
xvi
500 µm
xvii
100 µm
xviii

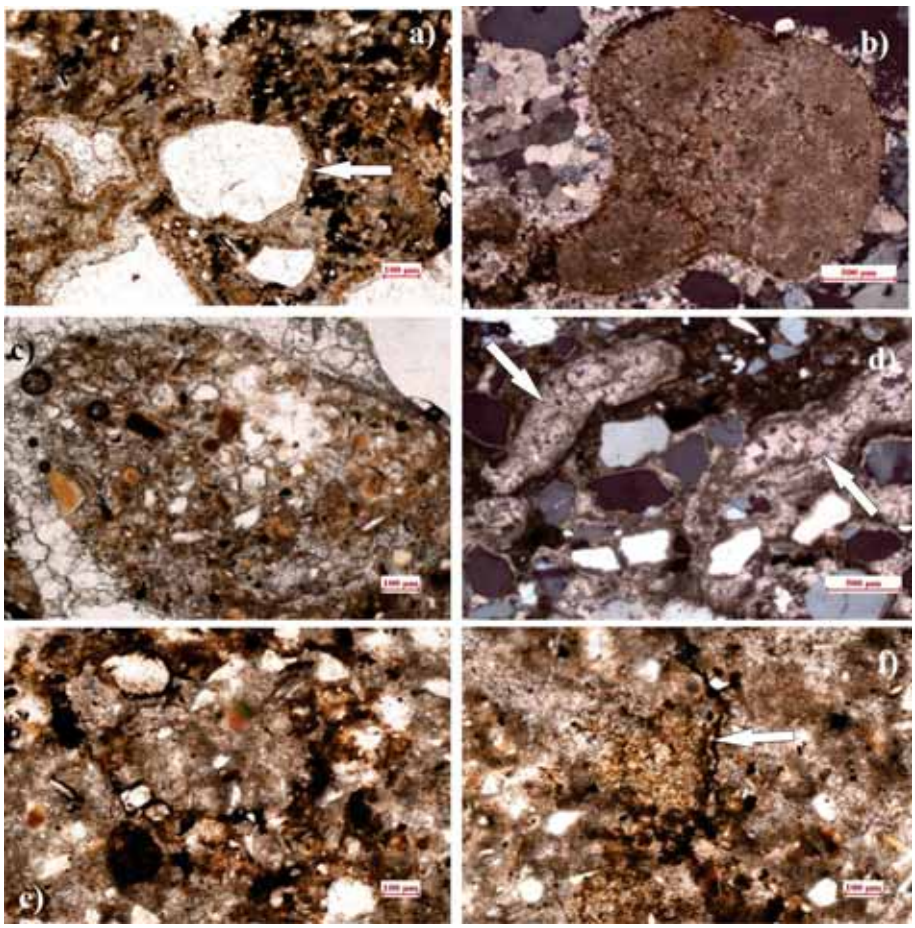

Figure 6. (**a**) Development of thin isopachous rim of clayey micrite surrounded by micritic calcite around the rounded quartz grain; surrounded by clayey micrite (PPL). (**b**) Mushroom shaped caliche nodule with discontinuous rim of micrite and carbonaceous clay, in turn surrounded by bladed blocky calcite rim (BCN). (**c**) Recycled caliche nodule containing framework grains with isopachous rim within the clayey micrite; the nodule is surrounded by bladed blocky calcite rim (PPL). (**d**) Fenestrae filled with sparry calcite. Note the fenestrae within the fenestrae in upper left part of photo (BCN). (**e**) Pedotubules consisting of pores lined with pale brownish clay (PPL). (**f**) Rhizoliths disrupting the original depostional texture and showing infiltration of clays along the root channel ways (PPL).

5. Discussion

Baneta Formation is represented by fining upward sequences of pebbly conglomerate, sandstone and siltstone. The lithofacies association observed in Baneta Formation, represents the mixed load meandering river deposits (Allen 1963, 1964, 1965, 1970; Reineck and Singh 1980; Reading 1981, 2006; Davis 1983; Miall 2006, 2014; Ghinassi *et al.* 2014; Garo *et al.* 2015). The thin, laterally discontinuous beds of polymict conglomerate represents the channel lag deposits formed under the conditions of lower flow regime (Allen 1964, 1970; Reading 1981, 2006; Miall 2006; Gazi and Mountney 2009). The overlying coarse- to fine-grained large scale tabular cross bedded sandstones represent the point bar deposits resulting from lateral accretion of stream bed load on sideward migration of meandering channels (Allen 1964, 1965; Jackson 1976; Yao *et al.* 2017). The horizontal parallel bedded sandstone indicates migration of plane beds near the point bar (Allen 1964; Miall 2006). The siltstone with intercalations of fine sandy layers, exhibiting parallel lamination, ripple lamination and climbing ripple lamination; represent vertically accreted overbank floodplain deposits (Reineck and Singh 1980; Reading 1981, 2006; Ghinassi *et al.* 2014; Miall 2014). Thin, discontinuous, tongue shaped lenses of better sorted coarse-grained sandstone with basal erosional contact and upper sharp contact, exhibiting ripple lamination and rhizoliths; represent the crevasse splay deposits (Allen 1964; O'Brian and Wells 1986; Reading 1981, 2006; Collinson 1996; Ghinassi *et al.* 2014). Hence, Baneta sediments are considered to represent channel lag, point bar and overbank floodplain deposits of mixed load meandering river. The observed intraformational calcareous conglomerate

Table 1. *Heavy mineral frequency percentages along with provenance sensitive indices (Morton and Hallsworth 1994, 1999; Morton and Milne 2012) of sediments of Baneta Formation.*

Sample No.	SG-1	SG-2	SG-3	SG-4	SG-5	CH-1	CH-2	CH-3	CH-4	CH-5	CH-6	Average
Minerals												
Zrn	2.43	3.25	2.15	2.09	2.58	2.14	2.75	2.07	1.96	2.44	1.71	2.32
Tur	1.05	1.12	0.95	0.83	3.55	0.88	1.52	0.96	0.88	1.68	0.94	1.31
Rt	0.60	0.56	0.32	0.28	0.97	0.34	0.44	0.38	0.62	0.37	0.34	0.47
Agt	88.69	87.22	88.32	88.55	79.35	84.03	85.25	86.86	87.22	84.93	85.36	85.98
Ep	0.22	0.24	0.32	0.14	0.32	0.24	1.64	0.84	0.42	0.23	0.78	0.49
St	0.22	0.24	–	–	0.65	2.03	1.46	1.11	2.23	1.52	2.70	1.11
Grt	4.02	3.66	4.98	3.07	5.48	5.46	3.56	4.24	4.61	5.87	6.52	4.68
Sil	0.38	0.40	0.50	0.28	–	0.25	0.40	0.27	0.31	0.20	0.35	0.30
Ky	0.46	0.52	0.41	0.14	0.65	1.65	0.20	0.18	0.24	0.15	0.47	0.46
Ttn	–	0.80	0.32	2.65	2.26	1.3	0.51	0.64	0.34	0.22	–	0.82
Zo	–	–	–	–	–	–	–	–	–	–	–	–
Spl	0.42	0.35	0.22	–	–	0.26	0.47	0.21	0.37	0.55	0.31	0.29
Chl	–	–	–	0.14	–	–	–	–	–	0.10	–	0.02
Mnz	0.22	0.24	–	–	0.32	0.12	0.18	–	–	0.10	0.12	0.12
Hbl	0.26	0.26	1.28	1.12	3.54	1.07	1.45	1.77	0.58	1.12	0.20	1.15
Ant	1.02	1.14	0.22	0.70	0.32	0.23	0.16	0.46	0.21	0.51	0.20	0.47
ZTR	4.08	4.93	3.42	3.20	7.10	3.36	4.71	3.41	3.46	4.49	2.99	4.10
PSI												
GZi	71.84	56.42	67.19	70.17	70.64	79.22	62.33	52.97	69.85	59.50	67.99	66.19
RZi	57.14	66.67	52.00	58.33	90.91	50.00	55.56	38.46	50.00	40.00	44.44	54.86
RuZi	13.71	13.79	15.51	24.03	13.17	16.59	19.80	14.70	12.96	11.81	27.32	16.67
Mzi	10.00	25.00	0.00	0.00	11.11	20.00	8.33	0.00	0.00	14.29	16.67	9.58
SZi	10.00	25.00	7.69	0.00	0.00	33.33	20.00	11.11	25.00	14.29	0.00	13.31
UTi	48.68	34.68	34.91	53.22	38.38	61.22	8.30	6.88	0.00	0.00	20.12	27.85
AmZRT	63.64	58.58	60.66	46.34	21.13	45.35	17.32	48.15	40.25	77.07	42.09	47.32
EpZRT	24.15	23.54	34.17	14.36	19.96	6.27	5.99	5.01	27.23	25.93	33.27	19.99
GtZRT	6.67	25.83	19.76	10.82	4.87	20.69	5.12	4.64	8.56	4.19	4.31	10.50
KyZRT	61.90	43.05	55.42	57.13	56.66	68.56	49.63	42.61	59.29	48.96	43.56	53.34

GZi	100 × garnet count/(total garnet + zircon)
RZi	100 × TiO_2 mineral count/(TiO_2 minerals + zircon)
RuZi	100 × rutile count/(rutile + zircon)
Mzi	100 × monazite count/(monazite + zircon)
SZi	100 × staurolite total/(staurolite + zircon)
UTi	100 × unstable total/(unstables + tourmaline)
AmZRT	Amphibole/(zircon + rutile + tourmaline + amphibole)
EpZRT	Epidote/(zircon + rutile + tourmaline + epidote)
GtZRT	100 × garnet count/(total garnet + zircon)
KyZRT	100 × TiO_2 mineral count/(TiO_2 minerals + zircon)

Zrn, Zircon; Tur, Tourmaline; Rt, Rutile; Agt, Augite; Ep, Epidote; St, Staurolite; Grt, Garnet; Sil, Sillimanite; Ky, Kyanite; Ttn-Sphene (Titanite); Zo, Zoisite; Spl, Spinel; Chl, Chlorite; Mnz, Monazite; Hbl, Hornblende; and Ant, Anatase; ZTR, Combined percentage of zircon; tourmaline and rutile; PSI, Provenance sensitive indices.

represent the reworked calcrete conglomerate (Khadkikar *et al.* 1998; Gomez-Gras and Alonso-Zarza 2003; Marriott and Wright 2006; Barclay *et al.* 2015); interpreted as channel-floor lag deposits of major channels that entered from distant uplands and drained the alluvial plain. Development of nodular calcrete, buckled bedded calcrete layers and rhizoliths, indicates semi-arid climatic conditions and related subaerial exposure of the Baneta sediments (Allen 1974; Leeder 1975; Reading 1981, 2006). Occasional development of calcrete-tepee structure suggests thermal and moisture related expansion–contraction in vadose zone under subaerial conditions (Eren 2007). The granulometric studies of the Baneta Formation support the fluvial deposition of these

Table 2. *Major oxide composition (wt.%) and weathering indices of sediments of Baneta Formation.*

Sample no.	BN-1	BN-5	BN-7	Average
Oxides				
SiO_2	63.78	71.41	51.13	62.10
Al_2O_3	2.40	4.48	12.21	6.37
TiO_2	0.35	0.39	1.84	0.86
Fe_2O_3	1.86	3.12	10.41	5.13
MnO	0.01	0.04	0.08	0.05
MgO	0.47	0.69	2.71	1.29
CaO	16.77	6.25	6.38	9.80
Na_2O	0.24	0.29	1.11	0.55
K_2O	0.64	0.80	1.05	0.83
P_2O_5	0.05	0.05	0.12	0.07
LOI	13.43	12.48	12.97	12.96
Sum	100.00	100.00	100.00	100.00
Weathering indices				
CIA	61.84	71.04	71.78	68.22
PIA	68.39	78.99	75.13	74.17
CIW	75.24	82.32	76.90	78.15
CIW′	85.87	90.30	86.94	87.70
ICV	1.80	1.37	1.70	1.62
WIP	11.61	24.91	23.25	19.92
W index	23.86	45.95	53.04	40.95

Table 3. *Trace and chondrite normalized* rare earth element composition (ppm) of sediments of Baneta Formation.*

Sample no.	BN-1	BN-5	BN-7	Average
Element				
Li	4.29	9.15	21.16	11.53
Be	2.17	3.68	7.69	4.51
Sc	5.12	8.20	24.01	12.44
Cr	52.30	74.77	243.70	123.59
V	24.07	40.21	92.49	52.26
Co	7.45	12.62	34.73	18.27
Ni	24.90	27.86	65.56	39.44
Cu	19.58	35.47	138.00	64.35
Zn	15.33	35.05	78.11	42.83
Ga	9.06	12.88	28.56	16.83
Sr	30.89	47.28	66.46	48.21
Rb	57.25	78.28	262.20	132.58
Cs	1.15	2.45	4.88	2.82
U	0.98	1.30	1.90	1.39
Ba	88.21	231.70	362.30	227.40
Th	4.75	6.39	7.34	6.16
Y	14.56	29.28	28.61	24.15
Zr	48.07	61.14	134.90	81.37
Nb	6.02	7.73	18.59	10.78
Sn	0.40	0.49	1.41	0.77
Sb	0.14	0.18	0.29	0.20
Pb	1.73	3.07	3.92	2.91
La	67.06	119.49	121.62	102.72
Ce	56.71	96.26	140.63	97.87
Pr	41.12	81.26	86.32	69.56
Nd	32.33	62.07	74.52	56.30
Sm	15.73	36.31	39.39	30.48
Eu	9.86	24.00	27.28	20.38
Gd	12.77	29.81	31.80	24.79
Tb	10.35	23.68	25.51	19.85
Dy	8.34	18.37	20.30	15.67
Ho	7.71	16.27	17.98	13.99
Er	8.19	16.02	17.96	14.06
Tm	7.84	14.48	17.08	13.13
Yb	7.43	12.74	15.96	12.04
Lu	7.44	12.32	15.24	11.67
ΣREE	292.87	563.06	651.59	502.51
La/Lu	9.01	9.70	7.98	8.90
Eu/Sm	0.63	0.66	0.69	0.66
Eu/Eu*	0.70	0.73	0.77	0.73
Ce/Ce*	1.08	0.98	1.37	1.14
La/Yb	9.03	9.38	7.62	8.68
La/Sm	4.26	3.29	3.09	3.55

*(Chondrite values after Lodders and Fegley 1998).

sediments (Reineck and Singh 1980; Reading 1981).

Lithic arenitic nature of Baneta sediments indicates their textural as well as mineralogical immaturity related with the nearness of source and short distance of transportation. The presence of subordinate amount of feldspars suggests their near source deposition and derivation from Deccan trap basalts and Precambrian granites, while presence of altered or replaced feldspars is indicative of warm climate during the deposition (Pettijohn 1984). The presence of varieties of polycrystalline quartz are inferred to be derived from quartzites and Precambrian gneisses (Young 1976; Blatt 1992). Presence of chert and fibrous chalcedony suggests the derivation from Deccan trap basalts while banded jasper suggests derivation from jasper bearing conglomerate of Bagra Formation of Gondwana Supergroup of Satpura Basin (Casshyap and Khan 2000). This variation in provenance is also seen from Dickinson's (1985) diagram (figure 4b). The variety of unstable lithic fragments such as siltstone, carbonaceous siltstone–sandstone and ferruginous sandstone are derived from Proterozoic Vindhyan Supergroup and Paleozoic Gondwana Supergroup sediments; granite, granodiorite, phyllite fragments suggest derivation from Precambrian Mahakoshal Group; mica gneiss fragment, detrital muscovite, and biotite represent the Precambrian unclassified basement gneissic provenance; varieties of basalts,

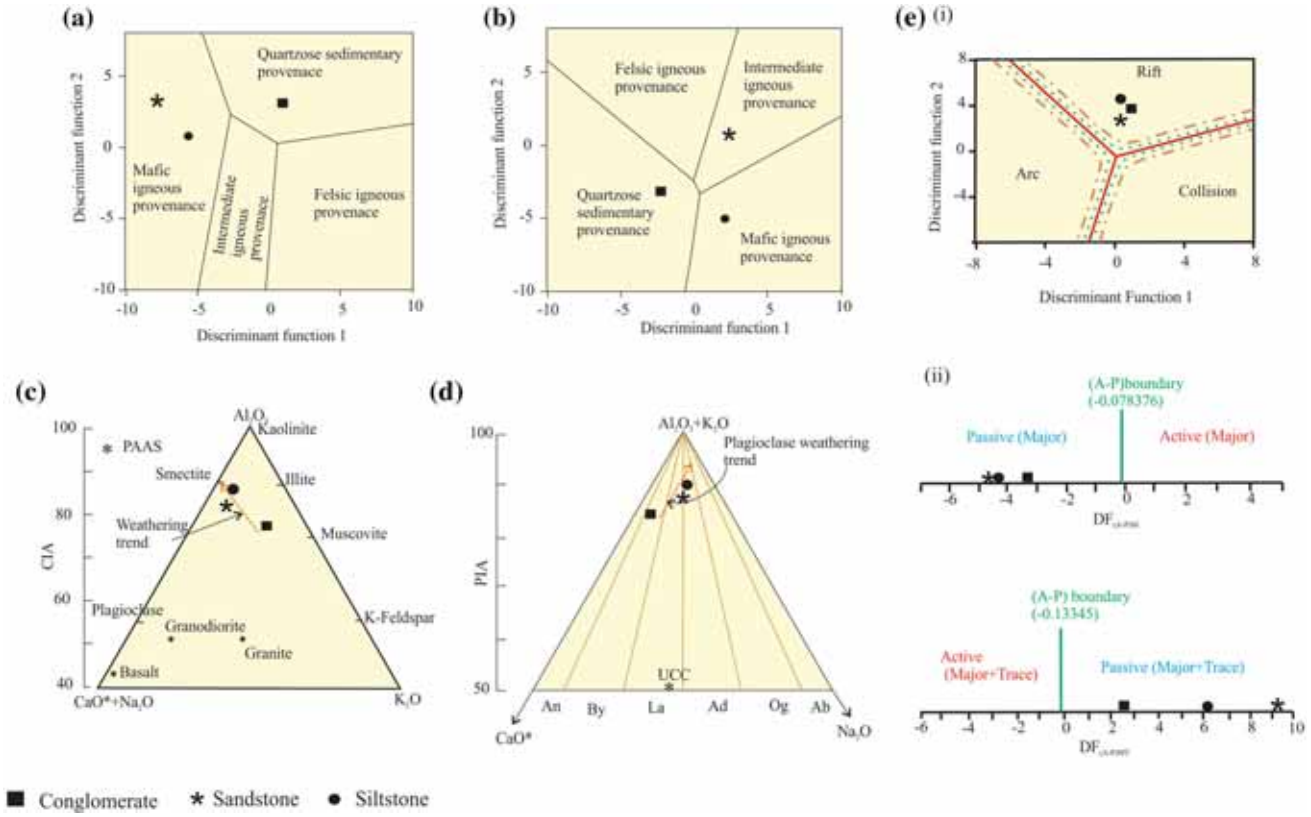

Figure 7. Discriminant function diagram for the provenance signatures of sediments from Baneta Formation using (**a**) major element ratios, (**b**) raw oxides (after Roser and Korsch 1988), (**c**) (Na_2O + CaO)–Al_2O_3–K_2O diagram showing the weathering trends (modified after Nesbitt and Young 1984, 1989; data for granite, basalt and granodiorite after Le Maitre 1976; Purevjav and Roser 2013). (**d**) CaO*–(Al_2O_3 + K_2O)–Na_2O diagram showing the weathering trends (modified after Nesbitt and Young 1982, positions of plagioclase feldspars after Purevjav and Roser 2013). An, By, La, Ad, Og, Ab – anorthite, bytownite, labradorite, andesine, oligoclase, and albite, respectively. (**e**) (i) Discriminant function multidimensional diagrams for sediments of Baneta Formation, the probability boundaries for 70% and 90% probabilities are also shown as dotted and dashed curves, respectively (after Verma and Armstrong-Altrin 2013), and (ii) major and trace element based multidimensional discriminant function diagrams of sediments of Baneta Formation (after Verma and Armstrong-Altrin 2016).

detrital pyroxene, volcanic glass and laterite clasts present in the thin sections of Baneta Formation are suggestive of derivation from Deccan trap basalts and lateritic cap; exposed to the east and southeast of study area (Jain *et al.* 1995). The framework constituents in all the thin sections are floating in unevenly distributed calcite cement. The presence of equant calcite rhombs coarsening towards pore centre producing interlocking mosaic, evenly distributed crystalline mosaic of blocky calcite and isopachous layers of bladed, blocky calcite crystals around the framework grains as well as around the micritic caliche nodules are considered to be formed in meteoric phreatic zone diagenetic environment (Longman 1980; Morse and Mackenzie 1990; Tucker and Wright 1990; Wright and Tucker 1991; Beckner and Mozley 1998; Hall *et al.* 2004; Wright 2007). Irregular and corroded borders of framework grains, circumgranular rims of micrite and/or microspar around grains, micritic calchie nodules, fenestrae, alveolar texture, and black carbonaceous clay infiltration are suggestive of meteoric vadose diagenesis and related subaerial exposure (Stenien 1974; Esteban and Klappa 1983; Purvis and Wright 1991; Bain and Foos 1993; Singh *et al.* 2007; Zhou and Chafetz 2009; Tanner 2010; Alonso-Zarza and Wright 2010; Eren *et al.* 2018). The irregular fenestrae result from root mats forming in zone of capillary rise (Semeniuk and Searle 1985; Wright *et al.* 1988; Beckner and Mozley 1998; Eren *et al.* 2018). The presence of carbonaceous clay in the caliche nodules as well as along the root channel ways are considered to be derived from overlying solum (Foos 1991). The mineralogical immaturity of Baneta sediments is further supported by their heavy mineral assemblage with low ZTR index and dominance of augite, indicating their derivation mainly from Deccan Trap Basalts. The derivation of these

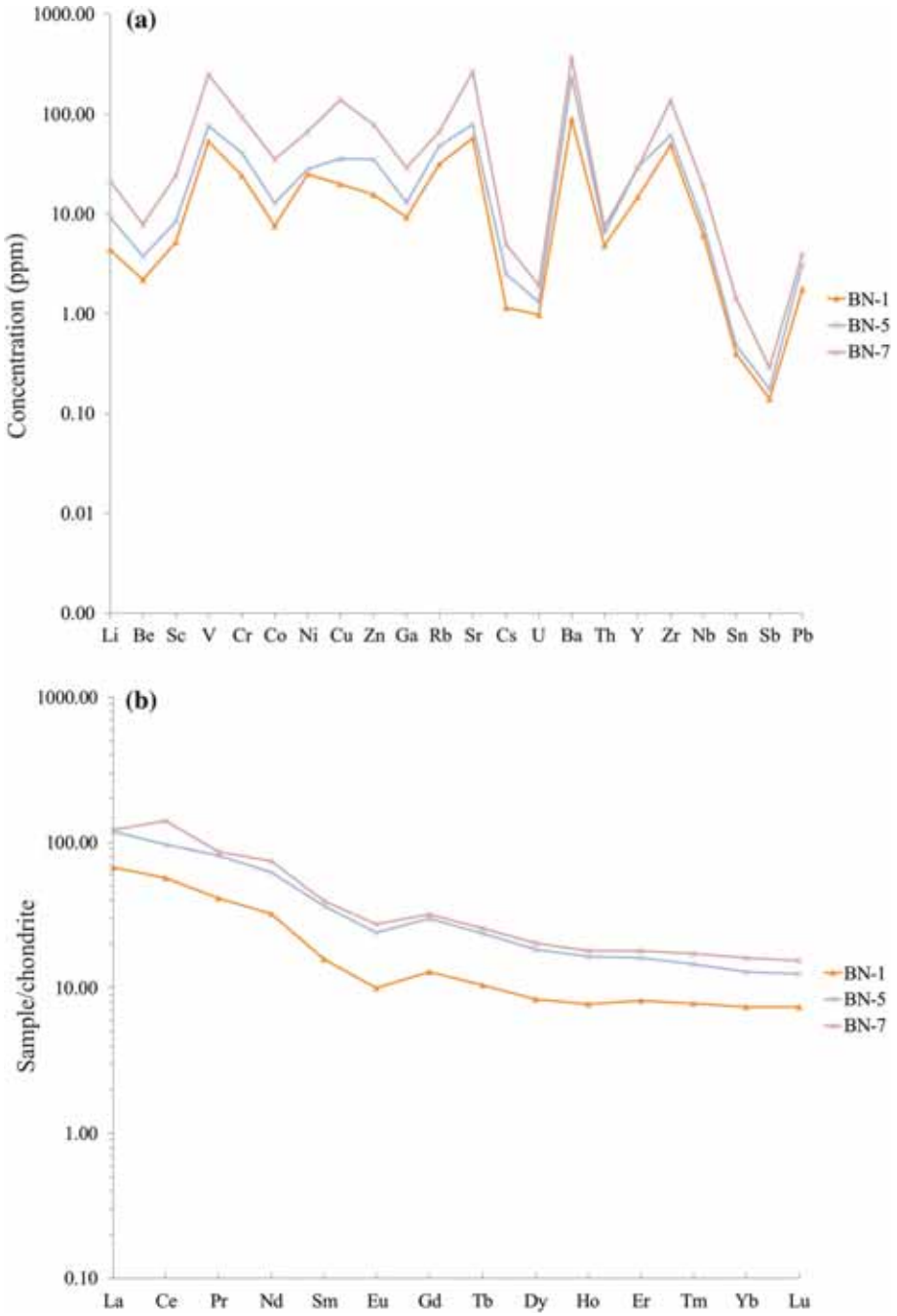

Figure 8. (**a**) Trace element distribution pattern in sediments of Baneta Formation. (**b**) Chondrite normalized rare earth element patterns of sediments of Baneta Formation.

sediments from Precambrian granites, ultramafics, metapelites and metabasic rocks exposed in the eastern, southern part of Narmada basin (Jain *et al.* 1995; Nair *et al.* 1995; Das *et al.* 2007) is supported by presence of epidote, staurolite, garnet, sillimanite, kyanite, sphene, spinel, zoisite, chlorite, monazite, hornblende, and anatase. The high values of GZi, RZi and GtZRT; moderate value of UTi, SZi and low values of RuZi, MZi, CZi, AmZRT, EpZRT, and KyZRT are suggestive of inputs from high grade metamorphic provenance, relatively more proportion of garnet compared to zircon and dominance of unstable heavy minerals (Morton and Hallsworth 1994; Ratcliffe *et al.* 2007). Montmorillonite is derived from the soils developed on Deccan Trap basalts, while illite and kaolinite are considered to be derived from Precambrian metapelite, granites of Mahakoshal Group and shales from Vindhyan and Gondwana Supergroups (Pettijohn 1984; Weaver

Table 4. *Stable isotopic composition of calcretes from sediments of Baneta Formation along with values of temperature (Freedman and O'Neil 1977) and pCO_2 (Cerling 1999; Arens et al. 2000).*

Sample no.	Type	$\delta^{13}C_{V\text{-}PDB}$	$\delta^{18}O_{V\text{-}PDB}$	T (°C)	pCO_2 (ppmV)
HB-4	Nodular calcrete	− 5.73	− 3.61	31.70	734.3
HB-2	Bedded calcrete	− 5.85	− 3.66	31.31	707.9
JH-2	Nodular calcrete	− 6.80	− 3.52	30.58	519.3
CH-9	Nodular calcrete	− 6.29	− 3.56	30.82	616.3
CH-8	Nodular calcrete	− 6.69	− 4.19	34.04	539.4
CH-6	Bedded calcrete	− 4.38	− 4.27	34.45	1081.0
CH-3B	Bedded calcrete	− 7.51	− 4.41	35.16	398.0
SG-5	Rhizolith	− 8.91	− 4.51	35.72	197.2
BNN-1	Bedded calcrete	− 7.53	− 4.16	33.84	394.8
BN-7	Nodular calcrete	− 5.40	− 2.39	25.09	810.1
BN-4	Nodular calcrete	− 4.37	− 3.32	29.61	1084.0
DO-3	Nodular calcrete	− 7.28	− 4.00	33.04	435.7
SU-3	Nodular calcrete	− 8.02	− 3.92	32.64	319.6
NP-10	Nodular calcrete	− 3.56	− 2.54	25.79	1349.7
Average		− 6.31	− 3.72	31.70	656.24

1989; Ahmad *et al.* 2012). This, coupled with southwesterly paleocurrent direction, supports the thin section studies of these sediments.

The high values of Fe_2O_3/K_2O and low values of Na_2O/K_2O indicate mineralogical immaturity of Baneta sediments owing to their lithic arenitic nature (Pettijohn *et al.* 1972; Herron 1988). The discriminant functions of Roser and Korsch (1988) support the mixed provenance of these sediments, as seen in petrographic and heavy mineral studies. CIA value of upper crust and fresh feldspars is 50 and increases up to 100 for highly weathered residual soils (Nesbitt and Young 1982; Fedo *et al.* 1995; Bahlburg and Dobrzinski 2009; Singh *et al.* 2016). Thus, CIA values of sediments of Baneta Formation (av. 68.33%) together with CIW′ (av. 87.80%), ICV (av. 1.62), W index (av. 40.95) and WIP (av. 19.92) are suggestive of varied provenance and indicate moderate weathering of the source in warm climate (Parker 1970; Cox *et al.* 1995; Ohta and Arai 2007; Xie *et al.* 2017). The sediments under study fall within the passive margin continental rift field on plot of Verma and Armstrong-Altrin (2013, 2016). The lithic arenitic nature of Baneta sediments hence can be linked with tectonic–climatic condition of the Central Narmada Basin (Ghosh 1976; Verma and Banerjee 1992).

According to Armstrong-Altrin *et al.* (2017), the trace elements such as Th, Sc, Cr and Co are used extensively for reconstructing the sediment provenance. Thorium content and Ba content of Baneta sediments is much higher than that of carbonates (Mason and Moore 1982) and hence indicate near source igneous provenance. Significant enrichment in Cr in these sediments compared to UCC (table 3) indicates contribution from mafic and ultramafic provenance (Armstrong-Altrin *et al.* 2013, 2017; Tetiker 2014). Major and trace element compositions of these sediments correspond closely to the composition of Deccan Trap basalts and dykes from Narmada Valley given by Mahoney (1988) and Sheth *et al.* (2009). Sr content of av. 48.21 ppm of these sediments is indicative of meteoric diagenesis of these sediments (Flugel 1982). Increase in LILE, HFSE, transition trace elements along with LREE in siltstone compared to sandstone and conglomerate may be attributed to concentration of heavy minerals in fine grained sediments compared to coarse-grained sediments.

REEs can be used as powerful tracers of geochemical processes to discover sources or provenance and its origin (Zhihua *et al.* 2003) as the REE patterns of the source rocks are preserved in clastic sediments (Taylor and McLennan 1985; Ali *et al.* 2014). The rare earth element composition of Baneta sediments show enrichment in LREE and depletion in HREE, with negative Eu anomaly reflecting the composition of upper continental crust (McLennan 1989). They exhibit low Eu/Sm ratio supporting their derivation from Deccan Trap basalts (Henderson 1984). Hence major, trace and rare earth element compositions of sediments of Baneta Formation are suggestive of their derivation mainly from Deccan Trap Basalt with minor contribution from other pre-Quaternary rocks in Narmada Basin (Roser and

Korsch 1988; Mahoney 1988; Sheth *et al.* 2009). The Ce anomaly is negligible in sandstone and conglomerate samples, and weakly positive in the siltstone (table 3), indicating adsorption or co-precipitation of CeO_2 on clay (Garzanti *et al.* 2011). This is well consistent with depletion in U (figure 8a) in oxic conditions and associated Ce scavenging (Garzanti *et al.* 2011). Weakly positive Ce anomaly is also linked with minor input from laterites (Sow *et al.* 2018) seen in thin section studies. Negative Eu anomaly also indicates selective adsorption of Eu on montmorillonite (Takahashi *et al.* 2004; Garzanti *et al.* 2011), thus supporting the basaltic provenance.

Carbonate stable isotopic compositions are important proxies of continental climate and environments (Godfray *et al.* 2018). The obtained values of $\delta^{13}C$ (av. − 6.31‰), and $\delta^{18}O$ (av. − 3.72‰) of the calcretes of Baneta Formation fit well within the range of world calcrete between –12 and +4 for $\delta^{13}C$ and –9 to +3 for $\delta^{18}O$ (Talma and Netterberg 1983; Salomans and Mook 1986a, b), and also within the isotopic range (+0.9 to −8.4‰) for average precipitation in North India (Sengupta and Sarkar 2006; Singh *et al.* 2016). The average $\delta^{18}O$ content of −3.72‰ suggest input of meteoric water and related meteoric diagenesis, as $\delta^{18}O$ of pedogenic carbonate is considered to be in equilibrium with that of soil water (Quade 1993), while isotopic composition of soil water is related to that of meteoric water (Khadkikar *et al.* 2000; Srivastava 2001; Singh *et al.* 2016). The obtained isotopic compositions of calcretes support pedogenic and/or shallow groundwater origin, vadose diagenetic conditions, related subaerial exposure for the calcretes under study (Cerling 1984; Beckner and Mozley 1998; Bajnoczi *et al.* 2006; Brlek and Glumec 2014), along with the fluctuating rainfall conditions in Central India (Tipple and Pagani 2007; Agrawal *et al.* 2012, 2014). $\delta^{13}C$ and $\delta^{18}O$ values, along with the average paleotemperatures of 31.70 °C and low pCO_2 (av. 656.24 ppmV), are suggestive of mixed paleovegetation cover of C3 (grain cereals, vegetables and woody trees) and C4 (mainly grasses and some monocotyledons), type plants with dominance of C4 plants and hence, a general hot climatic condition (Salomons and Mook 1986a, b; Quade *et al.* 1989; Purvis and Wright 1991; Wright *et al.* 1993; Tanner 2010; Li *et al.* 2013; Yamori *et al.* 2013; Eren *et al.* 2018; Godfray *et al.* 2018). According to Cerling *et al.* (1993), the dominance of C4 plants is primarily observed in tropical savannas, temperate grasslands and semi-desert scrublands. The stable isotopic values for calcretes of Baneta Formation thus indicate a Late Pleistocene landscape similar to temperate open grasslands in Central India (Patanaik *et al.* 2009; Verma and Rao 2011). The mollusc fossils found in floodplain siltstones of Baneta Formation are typical of freshwater stagnant pools, ponds, lakes and small sluggish streams (Subba Rao 1989).

Based on OSL date of sample from lower part of Narayanpur lithosection (NP-6: 83.72 ± 6.94 ka, measured in 2014 AD) and the sample from upper part of Chandla lithosection (CH-6B: 82.36 ± 8.06 ka, measured in 2014 AD), together with ^{14}C date of shells (BN-1 s: 22.63 ± 0.44 ^{14}C ka and SG-5s: 17.05 ± 0.93 ^{14}C ka); it can be inferred that the sediments of Baneta Formation were deposited in Late Pleistocene (Tiwari and Bhai 1997; Gibbard *et al.* 2010), during interstadial warm periods from MIS-5a to MIS-2 (Lisiecki and Raymo 2005). In western and central India, strong monsoon has been recorded from 100 to 70 ka followed by a dry phase from 70 to 60 ka (Singh *et al.* 1999, 2016; Srivastava *et al.* 2001; Chamyal *et al.* 2003; Kale 2003; Jain *et al.* 2004; Basu *et al.* 2018). The OSL date of NP-6 representing crevasse splay deposit thus suggests rise in flood intensities of Narmada River during the warm period of strong SW monsoon of interstadial MIS-5a (Schulz *et al.* 2002). The obtained stable isotope compositions and age data of calcretes from the study area matches with the monsoon variability recorded from fluvial sediments in NW India (Andrews *et al.* 1998; Jain and Tandon 2003; Juyal *et al.* 2006), in western India (Kale and Rajaguru 1987; Bhattacharya *et al.* 2017; Basu *et al.* 2018) and in central India (Singh *et al.* 1999; Srivastava *et al.* 2001). The observed development of calcretes in these sediments indicates pedogenesis, which is the characteristic feature of interstadial warm period (Dawson 1994).

6. Conclusion

To summarize, the sediments belonging to Baneta Formation represent the deposits of mixed load meandering rivers, derived from mixed provenance and undergone freshwater meteoric diagenesis related with semi-arid climate and subaerial exposure, based on:

- Fining upward sequences of pebbly conglomerate, sandstone and siltstone and their facies association, which are inferred to represent channel lag, point bar and overbank floodplain deposits of mixed load meandering river.

- The lithic arenitic nature of these sediments, low ZTR index along with predominance of augite; presence of illite, kaolinite and montmorillonite clays and geochemical compositions suggest; mineralogical immaturity of Baneta sediments derived from mixed provenance of Precambrian granite, metapelites, Vindhyan Supergroup; Gondwana Supergroup, Deccan trap basalt and laterite.
- The stable isotopic composition of calcretes and rhizoliths from Baneta Formation and calculated value of pCO_2 indicate meteoric digenesis under moderate to high paleotemperature related with subaerial exposure of sediments, with dominance of C4 type of paleovegetation and general warm climatic conditions in central India.
- The OSL and radiocarbon dates suggest that the sediments of Baneta Formation were deposited in Late Pleistocene Epoch, which corresponds to interstadial warm periods during MIS-5a stage to MIS-2 stage.

Acknowledgements

The first author is thankful to Department of Science and Technology (DST), New Delhi, for financial assistance (SR/S4/ES-477/2009). The authors thank Head, Department of Geology, Savitribai Phule Pune University, for providing necessary facilities during this work. The authors thank Dr K G Kulkarni, Agharkar Research Institute, Pune and Dr Shweta Gurav, St. Xavier's College, Mumbai, for help in fossil identification. We thank Drs Abhay Mudholkar, J N Pattan, and G Parthiban, from NIO, Goa, for providing major oxide and trace, REE data, respectively. Dr D J Patil, NGRI, Hyderabad, is thanked for providing C and O stable isotope data. We are thankful to Dr C M Nautiyal, Birbal Sahani Institute of Paleobotany, Lucknow, for extending radiocarbon dating facility. The authors are thankful to the anonymous reviewers for their constructive suggestions, which helped in improving the manuscript.

References

Agrawal S, Sanyal P, Sarkar A, Jaiswal M K and Dutta K 2012 Variability of Indian monsoonal rainfall over the past 100 ka and its implication for C3–C4 vegetational change; *Quat. Res.* **77** 159–170.

Agrawal S, Galy V, Sanyal P and Eglinton T 2014 C4 plant expansion in the Ganga Plain during the last glacial cycle: Insights from isotopic composition of vascular plant biomarkers; *Org. Geochem.* **67** 58–71.

Ahmad M, Srivastava S and Shrivastava J P 2012 REE abundance in the clays associated with the Intra-volcanic Bole Horizons of the Eastern Deccan Traps: Palaeoenvironmental implication; *Proc. India Nat. Sci. Acad.* **78** 59–69.

Aitken M J 1998 *Introduction to optical dating: The dating of quaternary sediments by the use of photon-stimulated luminescence*; Clarendon Press, Oxford, 282p.

Ali S, Stattegger K D, Garbe-Schönberg M, Frank M, Kraft S and Kuhnt W 2014 The provenance of Cretaceous to Quaternary sediments in the Tarfaya basin, SW Morocco: Evidence from trace element geochemistry and radiogenic Nd–Sr isotopes; *J. Afr. Earth Sci.* **90** 64–76.

Allen J R L 1963 The classification of cross stratified units, with notes on their origin; *Sedimentology* **2** 93–114.

Allen J R L 1964 Studies in fluviatile sedimentation: Six cyclothemes from the Lower Old Red Sandstone, Angola–Welsh basin; *Sedimentology* **3** 163–198.

Allen J R L 1965 A review of the origin and characteristics of recent alluvial sediments; *Sedimentology* **5** 80–191.

Allen J R L 1970 Studies in fluviatile sedimentation: A comparison of fining upward cyclothems with special reference to coarse member composition and interpretation; *J. Sedim. Petrol.* **40** 298–323.

Allen J R L 1974 Studies in fluviatile sedimentation: Lateral variation in some fining upwards cyclothems from the Red Marls Pembrokeshire; *J. Geol.* **9** 1–16.

Alonso-Zarza A M and Wright V P 2010 Calcretes; *Dev. Sedim.* **61** 225–267.

Andrews J E, Singhvi A K, Kailath J A, Kuhn R, Dennis P F, Tandon S K and Dhir R P 1998 Do stable isotope data from calcrete record late Pleistocene monsoonal climate variation in the Thar desert of India? *Quat. Res.* **50** 240–251.

Arens N C, Jahren A H and Amundson R 2000 Can C3 plants faithfully record the carbon isotopic composition of atmospheric carbon dioxide? *Paleobiol.* **26** 137–164.

Armstrong-Altrin J S, Nagarajan R, Madhavaraju J, Rosalez-Hoz L, Lee Y I, Balaram V, Cruz-Martinez A and Avila-Ramirez G 2013 Geochemistry of the Jurassic and upper Cretaceous shales from the Molango Region, Hidalgo, Eastern Mexico: Implications of source area weathering, provenance, and tectonic setting; *Com. Ren. Geosci.* **345** 185–202.

Armstrong-Altrin J S, Lee Y I, Kasper-Zubillaga J J and Trejo-Ramírez E 2017 Mineralogy and geochemistry of sands along the Manzanillo and El Carrizal beach areas, southern Mexico: Implications for palaeoweathering, provenance and tectonic setting; *Geol. J.* **52** 559–582.

Badam G L 1979 Quaternary palaeontology of the Central Narmada Valley and its implications in the prehistoric studies; *Geol. Surv. India, Misc. Publ.* **45** 311–320.

Badam G L 1983 A note on the discovery of upper Palaeolithic Culture from the Central Narmada Valley, Madhya Pradesh; *Curr. Sci.* **52** 976–978.

Bahlburg H and Dobrzinski A 2009 A review of the Chemical Index of Alteration (CIA) and its application to the study of Neoproterozoic glacial deposits and climate transitions; In:

The Geological Record of Neoproterozoic Glaciations (eds) Arnaud E, Halverson G P and Shields G A, *Geol. Soc. London, Memoirs*, **36** 81–93.

Bain R J and Foos A M 1993 Carbonate microfabrics related to subaerial exposure and paleosol formation; In: Carbonate Microfabrics (eds) Rezak R and Lavoi D L, *Front. Sedim. Geol.*, Springer-Verlag, New York, pp. 19–28.

Bajnoczi B, Horvath Z, Demney A and Mindszenty A 2006 Stable isotope geochemistry of calcrete nodules and septerian concretions in a Quaternary 'red clay' paleovertisol from Hungery; *Iso. Env. Heal. Stud.* **42** 335–350.

Banerjee A and Banerjee D M 2010 Modal analysis and geochemistry of two sandstones of the Bhander Group (Late Neoproterozoic) in parts of the Central Indian Vindhyan basin and their bearing on the provenance and tectonics; *J. Earth Syst. Sci.* **119** 825–839.

Barclay W J, Davis J R, Hiller R D and Waters R A 2015 Lithostratigraphy of Old red sandstone succession of Anglo-Welsh basin; *Tech. Report*, 106p.

Basu S, Sanyal P, Sahoo K, Chauhan N, Sarkar A and Juyal N 2018 Variation in monsoonal rainfall sources (Arabian Sea and Bay of Bengal) during the late Quaternary: Implications for regional vegetation and fluvial systems; *Palaeogeogr. Palaeoclimatol. Palaeoecol.* **491** 77–91.

Beckner J R and Mozley P S 1998 Origin and spatial distribution of early vadose and phreatic calcite cements in the Zia Formation, Albuquerque Basin, New Mexico, USA; In: Carbonate cementation in sandstones (ed.) Morad S, *Int. Assoc. Sedimentol.* **26** 27–51.

Bhandari S, Morya D M and Chamyal L S 2005 Late Pleistocene alluvial plain sedimentation in Lower Narmada Valley, western India: Paleoenvironmental implications; *J. Earth Syst. Sci.* **24** 433–444.

Bhattacharya F, Shukla A D, Patel R C, Rastogi B K and Juyal N 2017 Sedimentology, geochemistry and OSL dating of the alluvial succession in the northern Gujarat alluvial plain (western India): A record to evaluate the sensitivity of a semiarid fluvial system to the climatic and tectonic forcing since the late Marine Isotopic Stage 3; *Geomorphology* **297** 1–19.

Biswas S K, Basu P K and Sarkar G P 1989 Biostratigraphy of the Quaternary alluvial sediments in the Central Narmada basin and the middle Son basin in eastern M.P., Unpublished Report, *Geol. Surv. India*, 38p.

Blatt H 1992 *Sedimentary Petrology*; W.H. Freman and Co. Ltd., 2nd edn, 514p.

Bøtter-Jensen L, Andersen C E, Duller G A T and Murray A S 2003 Developments in radiation, stimulation and observation facilities in luminescence measurements; *Radiat. Meas.* **37** 535–541.

Brlek M and Glumec B 2014 Stable isotopic signatures of biogenic calcrete marking discontinuity surfaces: A case study from Upper Cretaceous carbonates of central Dalmatia and eastern Istria, Croatia; *Facies* **60** 773–788, https://doi.org/10.1007/s10347-014-0403-7.

Carver R E (ed.) 1971 *Procedures in Sedimentary Petrology*; John-Wiley and Sons, New York, 653p.

Casshyap S M and Khan A 2000 Tectono-sedimentary evolution of the Gondwana Satpura basin, central India: Evidence of pre-trap doming, rifting and paleoslope reversal; *J. Afr. Earth Sci.* **31** 65–76.

Cerling T E 1984 The stable isotopic composition of modern soil carbonate and its relationship to climate; *Earth Planet. Sci. Lett.* **71** 229–240.

Cerling T E 1999 Stable carbon isotopes in palaeosol carbonates; In: Palaeoweathering, palaeosurfaces and related continental deposits (eds) Thiry M and Simon-Coinçon R, *Int. Assoc. Sedimentol., Spec. Publ.* **27** 43–60.

Cerling T E, Wang Y and Quade J 1993 Expansion of C4 ecosystems as an indicator of global ecological change in the late Miocene; *Nature* **361** 344.

Chamyal L S and Juyal N 2008 Late Quaternary continental studies in parts of India: Implications for monsoon variability; *J. Geol. Soc. India* **71** 629–661.

Chamyal L S, Maurya D M, Bhandari S and Raj R 2002 Late Quaternary geomorphic evolution of the lower Narmada valley, western India: Implications for neotectonic activity along Narmada–Son Fault; *Geomorphology* **46** 177–202.

Chamyal L S, Maurya D M and Rachna R 2003 Fluvial systems of the drylands of western India: A synthesis of late Quaternary environmental and tectonic changes; *Quat. Int.* **04** 69–86.

Chauhan P R and Patnaik R 2008 The Narmada Basin Palaeoanthropology Project in central India; *Antiq.* **82** 317.

Choubey V D 1971 Narmada Son lineament, India; *Nat. Phys. Sci.* **55** 392–397.

Collinson J D 1996 Alluvial sediments; In: *Sedimentary Environments: Processes, Facies, and Stratigraphy* (ed.) Reading H G, Oxford, UK, Blackwell Science, pp. 37–82.

Collinson J, Mountney N and Thomson D 2006 *Sedimentary Structures;* Terra Publishing, England, 292p.

Cox R, Lowe D R and Cullers R L 1995 The influence of sediment recycling and basement composition on evolution of mudrock chemistry in the southwestern United States; *Geoch. Cosmoch. Acta* **59** 2919–2940.

Cullers R L 2000 The geochemistry of shales, siltstones and sandstones of Pennsylvanian–Permian age, Colorado, USA: Implications for provenance and metamorphic studies; *Lithos* **51** 181–203.

Das L K, Naskar D C, Roy K K, Majumdar R K, Choudhary R K and Srivastava S 2007 Crustal structure in central India from gravity and magnetotelluric data; *Curr. Sci.* **92** 200–208.

Davis R A Jr 1983 *Depositional systems: A genetic approach to sedimentary geology*; Prentice-Hall Inc., Englewood Cliffs, New Jersey, 669p.

Dawson A G 1994 *Ice age Earth: Late Quaternary Geology and Climate;* Routldge, London, New York, 316p.

De Terra H and Patterson T T 1939 *Studies on the Ice Age in India and Associated Human Culture*; Carnegie Institution of Washington Publication, 493p.

Dickinson W R 1985 Interpreting provenanace relations from detrital modes of sandstones; In: *Provenance of Arenites* (ed.) Zuffa G G, Reidel Dordrecht, pp. 333–361.

Ekart D D, Cerling T E, Montañez I P and Tabor N J 1999 A 400-million-year carbon isotope record of pedogenic carbonate: Implications for paleo atmospheric carbon dioxide; *Am. J. Sci.* **299** 805–827.

Eren M 2007 Genesis of tepees in the Quaternary hardpan calcretes, Mersin, S Turkey; *Carbonates and Evaporites* **22** 123–124.

Eren M, Kaplan M Y, Kadir S and Kapur S 2018 Biogenic (β-fabric) features in the hard-laminated crusts of the

Mersin and Adana regions, southern Turkey and the role of soil organisms in the formation of the calcrete profiles; *Catena,* https://doi.org/10.1016/j.catena.2017.12.021.

Esteban C M and Klappa C F 1983 Subaerial exposure environment; In: *Carbonate Depositional Environments*, *Mem. Am. Assoc. Pet. Geol.* **33** 1–54.

Fedo C M, Nesbitt H W and Young G M 1995 Unravelling the effects of potassium metasomatism in sedimentary rocks and paleosols, with implications for weathering conditions and provenance; *Geology* **23** 921–924.

Flugel E 1982 *Microfacies analysis of limestones*; Springer-Verlag, New York, 633p.

Foos A M 1991 Aluminous lateritic soils, Eleuthera Bacamas: A modern analog to carbonate Paleosols; *J. Sedim. Petrol.* **61** 340–348.

Friedman I and O'Neil J R 1977 Compilation of stable isotope fractionation factors of geochemical interest; In: *Data of Geochemistry* (ed.) Fleischer M, USGS Professional Paper 440 KK, pp. 1–12.

Galehouse J S 1971 Sedimentation analysis, In: *Procedures in Sedimentary Petrology* (ed.) Carver R E, John Wiley and Sons, New York, pp. 69–94.

Garo A I, Okosun E A, Salihu H A and Tenimu S 2015 Analysis of intermediate-scale reservoir heterogeneity based on well exposed outcrop analogue within the Maastrichtian Enagi Formation, Bida Basin, North Western Nigeria; *Uni. J. Geosci.* **3** 127–134.

Garzanti E, Andó S, France-Lanord C, Censi P, Vignola P, Galy V and Lupker M 2011 Mineralogical and chemical variability of fluvial sediments 2. Suspended-load silt (Ganga–Brahmaputra, Bangladesh); *Earth Planet. Sci. Lett.* **302** 107–120.

Gazi S and Mountney N P 2009 Facies and architectural element analysis of a meandering fluvial succession: The Permian Warchha Sandstone, Salt Range, Pakistan; *Sedim. Geol.* **221** 99–126.

Geological Survey of India 1993 Geological map of Son–Narmada–Tapti Lineament Zone, Central India, Special Project CRUMANSONATA, 1981–89, Unpublished Report, Geol. Surv. India.

Ghinassi M, Nemec W, Aldinucci M, Nehyba S, Ozaksoy V and Fidolini F 2014 Plan-form evolution of ancient meandering rivers reconstructed from longitudinal outcrop sections; *Sedimentology* **61** 952–977.

Ghosh D B 1976 The nature of Narmada Son Lineament; *Geol. Surv. India Misc. Publ.* **34** 119–133.

Gibbard P L, Head M J, Walker M J C and The Subcommision on Quaternary Stratigraphy 2010 Formal ratification of the Quaternary System/Period and Pleistocene Series/Epoch with a base at 2.58 Ma; *J. Quat. Sci.* **25** 96–102.

Godfray C, Fan M, Jesmok G, Upadhyay D and Tripati A 2018 Petrography and stable isotope geochemistry of Oligocene–Miocene continental carbonates in south Texas: Implications for paleoclimate and paleoenvironment near sea-level; *Sedim. Geol.,* https://doi.org/10.1016/j.sedgeo.2018.02.006.

Gómez-Gras D and Alonso-Zarza A M 2003 Reworked calcretes: Their significance in reconstruction of alluvial sequences (Permian and Triassic, Minorca, Balearic Islands, Spain); *Sedim. Geol.* **158** 299–319.

Hall J S, Mozley P, Davis J M and Roy N D 2004 Environments of formation and controls on spatial distribution of calcite cementation in Plio-Pleistocene fluvial deposits, New Mexico, USA; *J. Sedim. Res.* **74** 643–653.

Harnois L 1988 The CIW index: A new chemical index of weathering; *Sedim. Geol.* **55** 319–322.

Henderson P 1984 *Rare Earth Element Geochemistry*; Elsevier, Amsterdam, 510p.

Herron M M 1988 Geochemical classifications of terrigeneous sands and shales from Core to log data; *J. Sedim. Petrol.* **58** 820–829.

Hubert J F 1962 A zircon-tourmaline-rutile maturity index and the interdependence of the composition of heavy mineral assemblage with gross composition and the texture of sandstones. *J. Sedim. Petrol.* **32** 440–450.

Ingram R L 1971 Sieve analysis; In: *Procedures in Sedimentary Petrology* (ed.) Carver R E, John Wiley and Sons, New York, pp. 49–68.

Jackson R G 1976 Depositional model of point bars in the lower Wabash River; *J. Sedim. Petrol.* **46** 579–594.

Jafarzadeh M and Hosseini-Barzi M 2008 Petrography and geochemistry of Ahwaz Sandstone Member of Asmari Formation, Zagros, Iran: Implications on provenance and tectonic setting; *Rev. Mex. Cien. Geol.* **25** 247–260.

Jain S C, Nair K K K and Yedekar D B 1995 Geology of Son-Narmdada–Tapti lineament zone in Central India. In: *Geoscientific studies of Son–Narmada–Tapti Lineament zone* (eds) Jain S C, Yedekar D B, Chakrabarti N C, Nair K K K, Rao K V and Prasad V, Project CRUMANSONATA*, Geol. Surv. India, Spec. Publ.* **10** 1–154.

Jain M and Tandon S K 2003 Fluvial response to Late Quaternary climate changes, western India; *Quat. Sci. Rev.* **22** 2223–2235.

Jain M, Tandon S K and Bhatt S C 2004 Late Quaternary stratigraphic development in the lower Luni, Mahi and Sabarmati river basins, western India; *Proc. Indian Acad. Sci. (Earth. Planet. Sci.)* **113** 453–471.

Juyal N, Chamyal L S, Bhandari S, Bhushan R and Singhvi A K 2006 Continental record of the southwest monsoon during the last 130 ka: Evidence from the southern margin of the Thar Desert, India; *Quat. Sci. Rev.* **25** 2632–2650.

Kale V S 1986 The Narmada–Son structure A (Precambrian) reappraisal; Proceedings of Seminar 'Crustal Dynamics'; *India Geophys. Union, Hyderabad*, pp. 140–160.

Kale V S 2003 Geomorphic effects of monsoon floods on Indian rivers; In: *Flood Problem and Management in South Asia,* Springer, Dordrecht, pp. 65–84.

Kale V S and Rajaguru S N 1987 Late Quaternary alluvial history of the north-western Deccan upland region. *Nature* **325** 612–614.

Kathal P K 2018 Narmada: The longest westward flowing river of the peninsular India; In: *The Indian Rivers* (ed.) Singh D S, Springer, Singapore, pp. 301–308.

Khadkikar A S, Merh S S, Malik J N and Chamyal L S 1998 Calcretes in semi-arid alluvial systems: Formative pathways and sinks; *Sedim. Geol.* **116** 251–260.

Khadkikar A S, Chamyal L S and Ramesh R 2000 The character and genesis of calcretes in semi-arid to sub-humid alluvial systems and its bearing on the interpretation of ancient climates; *Palaeogeogr. Palaeoclimatol. Palaeoecol.* **142** 239–262.

Khan A A and Sonakia A 1992 Quaternary deposits of Narmada with special reference to Hominid fossils; *J. Geol. Soc. India* **39** 147–154.

Kotlia B S and Joshi M 2008 Reconstruction of Late Pleistocene palaeoecology of the Upper Narmada valley (central India) using fossil communities; *Palaeoworld* **17** 153–159.

Laskar A H, Sharma N, Ramesh R, Jani R A and Yadava M G 2010 Paleoclimate and paleovegetation of Lower Narmada Basin, Gujarat, western India, inferred from stable carbon and oxygen isotopes; *Quat. Int.* **227** 183–189.

Le Maitre R W 1976 The chemical variability of some common igneous rocks; *J. Petrol.* **17** 589–598.

Leeder M R 1975 Pedogenic carbonate and flood sediment accretion rates: A quantitative model for alluvial arid zone lithofacies; *Geol. Mag.* **112** 257– 270.

Li X, Jenkyns H C, Zhang C, Wang Y, Liu L and Cao K 2013 Carbon isotope signatures of pedogenic carbonates from SE China: Rapid atmospheric pCO_2 changes during middle–late Early Cretaceous time; *Geol. Mag.* **151** 1–20.

Lisiecki L E and Raymo M E 2005 A Pliocene–Pleistocene stack of 57 globally distributed benthic ^{18}O records; *Paleooceanogr. Paleoclimatol.* **2** 1–17.

Lodders K and Fegley B 1998 *The planetary scientist's companion*; Oxford University Press, 400p.

Longman M W 1980 Carbonate diagenetic texture from near surface diagenetic environments; *Bull. Am. Assoc. Petrol. Geol.* **64** 461–487.

Mahoney J J 1988 Deccan Traps; In: *Continental Flood Basalts* (ed.) Macdougall J D, Kluwer Academic Press, pp. 151–194.

Marriott S B and Wright V P 2006 Investigating paleosol completeness and preservation in mid Paleozoic alluvial paleosol: A case study in paleosol taphonomy from Lower Old Red Sandstone; *Geol. Soc. Am. Spec. Paper* **416** 43–52.

Mason B and Moore C B 1982 *Principles of Geochemistry*; John Wiley and Sons, New York, 344p.

McLennan S M 1989 Rare earth elements in sedimentary rocks: Influence of provenance and sedimentary processes; *Rev. Mineral.* **21** 169–200.

Miall A D 2006 *The geology of fluvial deposits sedimentary facies, basin analysis, and petroleum geology;* Springer-Verlag, Berlin, Heidelberg, 582p.

Miall A D 2014 fluvial depositional systems; Springer, Netherlands, 316p.

Mishra D C 2015 Plume and Plate tectonics model for formation of some Proterozoic basins of India, along contemporary mobile belts: Mahakoshal-Bijawar, Vindhyan and Cuddapah basins; *J. Geol. Soc. India* **85** 525–536.

Morse J W and Mackenzie F T 1990 Geochemistry of sedimentary carbonates; Elsevier Amsterdam, New York, *Dev. Sedim.* **48** 707.

Morton A C and Hallsworth C R 1994 Identifying provenance-specific features of detrital heavy mineral assemblages in sandstones; *Sedim. Geol.* **90** 241–256.

Morton A C and Hallsworth C R 1999 Processes controlling the composition of heavy mineral assemblages in sandstones; *Sedim. Geol.* **124** 3–29.

Morton A and Milne A 2012 Heavy mineral stratigraphic analysis on the Clair Field, UK, west of Shetlands: A unique real-time solution for red-bed correlation while drilling; *Petrol. Geosci.* **18** 115–128.

Nair K K K, Jain S C and Yedekar D B 1995 Stratigraphy, structure and geochemistry of Mahakoshal greenstone belt; *Geol. Soc. India, Memoir* **31** 403–432.

Nautiyal C M 2012 Radiocarbon dating in determining the antiquity of cultural remains in India; In: *Era Historicity of Vedic and Ramayan. I-SERVE* (eds) Saroj Bala and Kulbhushan Mishra, Delhi, pp. 125–142.

Nesbitt H W and Young G M 1982 Early Proterozoic climates and plate motions inferred from major element chemistry of lutites; *Nature* **299** 715–717.

Nesbitt H W and Young G M 1984 Prediction of some weathering trends of plutonic and volcanic rocks based on thermodynamic and kinetic considerations; *Geochim. Cosmochim. Acta* **48** 1523–1534.

Nesbitt H W and Young G M 1989 Formation and diagenesis of weathering profiles; *J. Geol.* **97** 129–147.

O'Brian P E and Wells A T 1986 A small alluvial crevasse splay; *J. Sedim. Petrol.* **56** 876–879.

Ohta T and Arai H 2007 Statistical empirical index of chemical weathering in igneous rocks: A new tool for evaluating the degree of weathering; *Chem. Geol.* **240** 280–297.

Okada H 1971 Classification of sandstone: Analysis and proposal; *J. Geol.* **79** 509–525.

Parker A 1970 An index of weathering for silicate rocks; *Geol. Mag.* **107** 501–504.

Patnaik R, Chauhan P R, Rao M R, Blackwell B A B, Skinner A R, Sahni A, Chauhan M S and Khan H S 2009 New geochronological, paleoclimatological, and archaeological data from the Narmada Valley hominin locality, central India; *J. Hum. Evol.* **56** 114–133.

Patro B P K, Harinarayana T, Sastry R S, Rao M, Manoj C, Naganjaneyulu K and Sarma S V S 2005 Electrical imaging of Narmada–Son Lineament Zone, central India from magnetotellurics; *Phys. Earth Planet. Int.* **148** 215–232.

Pettijohn E J 1984 *Sedimentary Rocks*; CBS Publishers and Distributors, Delhi, 628p.

Pettijohn F J, Potter P E and Siever R 1972 *Sand and sandstones*; Springer-Verlag, New York, 547p.

Purevjav N and Roser B 2013 Geochemistry of Silurian–Carboniferous sedimentary rocks of the Ulaanbaatar terrane, Hangay–Hentey belt, central Mongolia: Provenance, paleoweathering, tectonic setting, and relationship with the neighbouring Tsetserleg terrane; *Chemie der Erde* **73** 481–493.

Purvis K and Wright V P 1991 Calcretes related to phreatophytic vegetation from Middle Triassic Otter Sandstone of South west England; *Sedimentology* **38** 539–551.

Quade J 1993 Stable carbon and oxygen isotopes in soil carbonates: Climate change in continental isotopic records. *Geophys. Monogr.* **78** 217–231.

Quade J, Cerling T E and Bowman J R 1989 Development of monsoon revealed by marked ecological shift during the latest Miocene in the northern Pakistan; *Nature* **342** 163–166.

Raj R 2008 Occuence of volcanic ash in the Quaternary alluvial deposits Lower Narmada basin western India; *J. Earth Syst. Sci.* **117** 41–48.

Ratcliffe K T, Morton A C, Ritcey D H and Evenchik C A 2007 Whole-rock geochemistry and heavy mineral analysis as petroleum exploration tools in the Bowser and Sustut basins, British Columbia, Canada; *Bull. Can. Petrol. Geol.* **55** 320–336.

Reading H Q 1981 *Sedimentary Environments and Facies;* Blackwell Scientific Publications, Oxford, London, 569p.

Reading H Q 2006 *Sedimentary Environments: Processes, Facies, and Stratigraphy*; Blackwell Publishing, India, 688p.

Reineck H E and Singh I B 1980 *Depositional Sedimentary Environments*; Springer-Verlag, Berlin, Heidelburg, New York, 549p.

Robinson S A, Andrew S J E, Hesselbo S P, Radley J D, Dennis P F, Harding I C and Allen P 2002 Atmospheric pCO_2 and depositional environment from stable-isotope geochemistry of calcrete nodules (Barremian, Lower Cretaceous, Wealden Beds, England); *J. Geol. Soc.* **159** 215–224.

Roser B P and Korsch R J 1988 Provenance signatures of sandstone–mudstone suites determined using discriminant function analysis of major of major element data; *Chem. Geol.* **67** 119–139.

Salomons W and Mook W G 1986a Isotope geochemistry of carbonate dissolution and reprecipitation in soils; *Soil. Sci.* **122** 15–24.

Salmons W and Mook W G 1986b Isotope geochemistry of carbonates in weathering zone; In: *Handbook of Environmental Isotope Geochemistry* (eds) Fritz P and Frontes J Ch, New York, 2 239–269.

Sankhyan A R 2017 First record and study of prehistoric sacra from central Narmada valley (MP); *Int. J. Anat. Res.* **5** 4144–4151.

Sankyan A R, Dewangan L N, Chakraborty S, Kundu S, Prabha S, Chakravarty R and Badam G L 2012 New human fossils and associated findings from the Central Narmada Valley, India; *Curr. Sci.* **103** 1461–1469.

Schulz H, Emeis K C, Erlenkeuser H, von Rad U and Rolf C 2002 The Toba volcanic event and interstadial/stadial climates at the marine isotopic stage 5 to 4 transition in the northern Indian Ocean; *Quat. Res.* **57** 22–31.

Semeniuk V and Searle D J 1985 Distribution of calcrete in Holocene coastal sands in relationship to climate, southwestern Australia; *J. Sedim. Petrol.* **56** 86–95.

Sengupta S and Sarkar A 2006 Stable isotope evidence of dual (Arabian Sea and Bay of Bengal) vapor sources in monsoonal precipitation over north India; *Earth Planet. Sci. Lett.* **250** 511–521.

Sheth H C, Ray J S, Ray R, Vanderkluysen L, Mahoney J J, Kumar A, Shukla A D, Das P, Adhikari S and Jana B 2009 Geology and geochemistry of Pachmarhi dykes and sills, Satpura Gondwana basin, central India: Problems of dikes-sill-flow correlation in the Deccan Traps; *Contrib. Mineral. Petrol.* **158** 357–380.

Singh I B, Sharma S, Sharma M, Srivastava P and Rajagopalan G 1999 Evidence of human occupation and humid climate of 30 ka in the alluvium of southern Ganga Plain; *Curr. Sci.* **76** 1022–1026.

Singh B P, Lee Y I, Pawar J S and Charak R S 2007 Biogenic features in calcretes developed on mudstone: Examples from Paleogene sequences of the Himalaya, India; *Sedim. Geol.* **201** 149–156.

Singh A, Paul D, Sinha R, Thomsen K J and Gupta S 2016 Geochemistry of buried river sediments from Ghaggar Plains, NW India: Multi-proxy records of variations in provenance, paleoclimate, and paleovegetation patterns in the Late Quaternary; *Palaeogeogr. Palaeoclimatol. Palaeoecol.* **449** 85–100, https://doi.org/10.1016/j.palaeo.2016.02.012.

Sonakia A 1984 The skull cap of Early man and associated mammalian fauna from Narmada Valley alluvium, Hoshangabad area, M.P., India; *Rec. Geol. Surv. India* **113** 159–172.

Sow M A, Payre-Suc V, Julien F, Camara M, Baque D, Probst A and Probst J L 2018 Geochemical composition of fluvial sediments in the Milo River basin (Guinea): Is there any impact of artisanal mining and of a big African city, Kankan? *J. Afr. Earth Sci.* **145** 102–114.

Splishbury C G 1833 Account of the bones discovered in beds of the Omar Nadi Near Narsingpur in the valley of Nerbuda; *J. Asiatic Soc. Bengal* **2** 388–395.

Srivastava P 2001 Paleoclimatic implications of pedogenic carbonates in Holocene soils of Gangatic plains, India; *Palaeogeogr. Palaeoclimatol. Palaeoecol.* **172** 207–222.

Srivastava P, Juyal N, Singhvi A K, Wasson R J and Bateman D 2001 Luminescence chronology of river adjustment and incision of Quaternary sediments in the alluvial plain of Sabarmati river, north Gujarat, India; *Geomorphology* **36** 217–229.

Stenien R P 1974 Phreatic and vadose diagenetic modification of Pleistocene limestone: Petrographic observations from subsurface of Barbados, West Indies; *Bull. Am. Assoc. Petrol. Geol.* **58** 1008–1024.

Subba Rao N V 1989 *Handbook of freshwater molluscs of India*; Zoological Survey of India Publications, 289p.

Takahashi Y, Tada A and Shimizu H 2004 Distribution pattern of rare earth ions between water and montmorillonite and its relation to the sorbed species of the ions; *Anal. Sci.* **20** 1301–1306.

Talma A S and Netterberg F 1983 Stable isotope abundances in calcretes; *Geol. Soc. London, Spec. Publ.* **11** 221–233.

Tanner L H 2010 Continental carbonates as indicators of paleoclimate; In: Carbonates in continental settings: Geochemistry, diagenesis and applications (eds) Alonso-Zarza A M and Tanner L H, *Dev. Sedim.* **62** 179–206.

Taylor S R and Mclennan S M 1985 *The continental crust: Its composition and evolution*; Blackwell, London, 311p.

Tetiker S 2014 Petrography and geochemistry of Early Palaeozoic clastic rocks from the southeast Anatolian autochthone rocks in Mardin area (Derik-Kiziltepe), Turkey; *Carpath. J. Earth. Env.* **9** 149–162.

Theobald W 1860 On Tertiary and alluvial deposits of the central Narmada Valley; *Geol. Surv. India, Memoir* **2** 279–298.

Tipple B J and Pagani M 2007 The early origins of terrestrial C4 photosynthesis; *Ann. Rev. Earth Planet. Sci.* **35** 435–461.

Tiwari M P 2007 Correlation of lithostratigraphy and chronology of the Narmada Valley Quaternary; In: *Human Origins, Genome and People of India: Genomic, Paleontological and Archaeological Perspectives* (eds) Sankhyan A R and Rao V R, Allied Publisher Private Limited, Mumbai, pp. 165–174.

Tiwari M P and Bhai H Y 1997 Quaternary stratigraphy of the Narmada Valley; *Geol. Surv. India, Spec. Publ.* **46** 33–63.

Tripathi C 1968 The Pleistocene alluvial deposits of central India; *Rec. Geol. Surv. India*, 95p.

Tucker M E and Wright V P 1990 *Carbonate Sedimentology*; Blackwell Scientific Publications, Oxford, London, 482p.

Vaidyanathan R and Ramakrishnan M 2008 *Geology of India*; Geological Society of India (Vol. 2), pp. 833–906.

Venkata Rao K, Chakraborti S, Rao K J, Ramani M S V, Marathe S D and Borkar B T 1997 Magnetostratigraphy of the Quaternary fluvial sediments and tephra of Narmada valley, central India; *Geol. Surv. India Spec. Publ.* **48** 65–78.

Verma S P and Amstrong-Altrin J S 2013 New multi-dimensional diagrams for tectonic discrimination of siliciclastic sediments and their application to Precambrian basins; *Chem. Geol.* **355** 117–133.

Verma S P and Armstrong-Altrin J S 2016 Geochemical discrimination of siliciclastic sediments from active and passive margin settings; *Sedim. Geol.* **332** 1–12.

Verma R K and Banarjee P 1992 Nature of continental crust along the Narmada–Son Lineament, inferred from gravity and deep seismic sounding data; *Tectonophys.* **202** 375–397.

Verma P and Rao M R 2011 Quaternary vegetation and climate change in Central Narmada Valley: Palynological records from hominin bearing sedimentary successions; In: *Geological processes and climate change* (eds) Singh D N and Chabbra L S, Macmillan Publishers India Pvt. Ltd., pp. 71–84.

Visher G S 1969 Grain size distribution and depositional processes; *J. Sedim. Petrol.* **49** 41– 62.

Weaver C E 1989 *Clays, muds and shales*; Elsevier Science Publishing Company Inc., New York, 819p.

Wintle A G and Murray A S 2000 Quartz OSL: Effects of thermal treatment and their relevance to laboratory dating procedures; *Radiat. Meas.* **32** 387–400.

Wright V P 2007 Calcretes; In: *Geochemical sediments and landscapes* (eds) Nash D and McLaren S, Willey-Blackwell, pp. 10–45.

Wright V P and Tucker M E 1991 Calcretes, International Association of Sedimentologists Reprint Series, 352p.

Wright V P, Turner M S, Andrews J E and Spiro B 1993 Morphology and significance of supermature calcretes from the Upper Old Red Sandstone of Scotland; *J. Geol. Soc. London* **150** 871–883.

Wright V P, Platt N H and Wimbledon W A 1988 Biogenic laminar calcretes: Evidence of calcified root-mat horizons in paleosols; *Sedimentology* **35** 603–620.

Xie Y, Yuan F, Zhan T, Kang C and Chi Y 2017 Geochemical and isotopic characteristics of sediments for the Hulun Buir Sandy Land, northeast China: Implication for weathering, recycling and dust provenance; *Catena* **160** 170–184.

Yamori W, Hikosaka K and Way D A 2013 Temperature response of photosynthesisin C3, C4 and CAM plants: Temperature acclimation and temperature adaptation; *Photo. Res.* **119** 101–117, https://doi.org/10.1007/s11120-013-9874-6.

Yao Z, Yu X, Shan X, Li S, Li S, Li Y, Tan C and Chen H 2017 Braided–meandering system evolution in the rock record: Implications for climate control on the Middle–Upper Jurassic in the southern Junggar Basin, north-west China; *Geol. J.*, https://doi.org/10.1002/gj.3105.

Young W S 1976 Petrographic textures of detrital polycrystalline quartz as an aid to interpret crystalline source rock; *J. Sedim. Petrol.* **46** 595–603.

Zhihua C, Gao A Yanguang L, Haiquing S Xuefa S and Zuosheng Y 2003 REE geochemistry of surface sediments in the Chukchi Sea; *Science in China Series D: Earth Sci.* **46** 603–611.

Zhou J and Chafetz H S 2009 The genesis of late Quaternary caliche nodules in Mission Bay, Texas: Stable isotopic compositions and palaeoenvironmental interpretation; *Sedim. Geol.* **222** 207–225.

Corresponding editor: Santanu Banerjee